Impairment of starvation-induced and constitutive autophagy in *Atg7*-deficient mice

MASAAKI KOMATSU, SATOSHI WAGURI, TAKASHI UENO, JUNICHI IWATA, SHIGEO MURATA, ISEI TANIDA, JUNJI EZAKI, NOBORU MIZUSHIMA, YOSHINORI OHSUMI, YASUO UCHIYAMA, EIKI KOMINAMI, KEIJI TANAKA, and TOMOKI CHIBA

Reprinted From: The Journal of Cell Biology
Volume 169 Number 3 May 9, 2005

Impairment of starvation-induced and constitutive autophagy in *Atg7*-deficient mice

Masaaki Komatsu,[1,3] Satoshi Waguri,[2] Takashi Ueno,[3] Junichi Iwata,[3] Shigeo Murata,[1] Isei Tanida,[3] Junji Ezaki,[3] Noboru Mizushima,[4] Yoshinori Ohsumi,[5] Yasuo Uchiyama,[2] Eiki Kominami,[3] Keiji Tanaka,[1] and Tomoki Chiba[1]

[1]Department of Molecular Oncology, Tokyo Metropolitan Institute of Medical Science, Bunkyo-ku, Tokyo 113-8613, Japan
[2]Department of Cell Biology and Neurosciences, Osaka University Graduate School of Medicine, Osaka 565-0871, Japan
[3]Department of Biochemistry, Juntendo University School of Medicine, Bunkyo-ku, Tokyo 113-8421, Japan
[4]Department of Bioregulation and Metabolism, Tokyo Metropolitan Institute of Medical Science, Bunkyo-ku, Tokyo 113-8613, Japan
[5]Department of Cell Biology, National Institute for Basic Biology, Okazaki 444-8585, Japan

Autophagy is a membrane-trafficking mechanism that delivers cytoplasmic constituents into the lysosome/vacuole for bulk protein degradation. This mechanism is involved in the preservation of nutrients under starvation condition as well as the normal turnover of cytoplasmic component. Aberrant autophagy has been reported in several neurodegenerative disorders, hepatitis, and myopathies. Here, we generated conditional knockout mice of *Atg7*, an essential gene for autophagy in yeast. *Atg7* was essential for ATG conjugation systems and autophagosome formation, amino acid supply in neonates, and starvation-induced bulk degradation of proteins and organelles in mice. Furthermore, *Atg7* deficiency led to multiple cellular abnormalities, such as appearance of concentric membranous structure and deformed mitochondria, and accumulation of ubiquitin-positive aggregates. Our results indicate the important role of autophagy in starvation response and the quality control of proteins and organelles in quiescent cells.

Introduction

There are two major protein degradation pathways in eukaryotic cells: the proteasome and the lysosome. The proteasome is a self-compartmentalized protease complex with catalytic activities inside its central proteinaceous chamber (Baumeister et al., 1998). It plays crucial roles in selective degradation of not only short-lived regulatory proteins but also abnormal proteins that should be eliminated from the cells (Goldberg, 2003). In contrast, the lysosome is a vesicle that contains many hydrolases, which are separated from the cytosol by the limiting membrane. In this lysosomal pathway, degradation of plasma membrane proteins and extracellular proteins is mediated by endocytosis, whereas degradation of cytoplasmic components is achieved through several pathways: macroautophagy, microautophagy, and chaperone-mediated autophagy (Seglen and Bohley, 1992; Dunn, 1994; Klionsky and Emr, 2000; Massey et al., 2004).

Macroautophagy (hereafter referred to as autophagy) is the main route for sequestration of the cytoplasm into the lysosome. The initial step of autophagy is elongation of the isolation membrane. The isolation membrane initially enwraps cytoplasmic constituents such as organelles, and then its edges fuse with each other forming a double membrane structure called autophagosome. Finally, the outer membrane of the autophagosome fuses with the lysosome/vacuole and the sequestered cytoplasmic components are degraded by the lysosomal/vacuolar hydrolases, together with the inner membrane of the autophagosomes (Mizushima et al., 2002).

In mammals, autophagy is considered necessary for the turnover of cellular components, particularly in response to starvation or glucagons (Mortimore and Poso, 1987). Yeast deficient in autophagy rapidly die under nutrition-poor conditions (Tsukada and Ohsumi, 1993), suggesting its important roles in preservation of nutrient supply. Indeed, autophagy is necessary for survival in early neonatal starvation period in mice (Kuma et al., 2004). Furthermore, autophagy plays a role in cellular remodeling during differentiation and development of multicellular organisms, such as fly, worm, and slime mold (Levine and Klionsky, 2004), and cellular defense against invading streptococcus (Nakagawa et al., 2004). Plants deficient in autophagy show accelerated senescence (Hanaoka et al., 2002). In humans, autophagy has been implicated in several pathological conditions (Shintani and Klionsky, 2004); e.g., low levels of autophagy were described in some malignant tumors (Liang et al., 1999).

Correspondence to Tomoki Chiba: tchiba@rinshoken.or.jp

Abbreviations used in this paper: MEF, mouse embryonic fibroblast; plpC, polyinosinic acid–polycytidylic acid; PNS, postnuclear supernatant; SDH, succinate dehydrogenase.

The online version of this article includes supplemental material.

The Journal of Cell Biology, Vol. 169, No. 3, May 9, 2005 425–434
http://www.jcb.org/cgi/doi/10.1083/jcb.200412022

In contrast, elevated levels of autophagosome formation were reported in other human pathologies such as neurodegenerative diseases, myopathies, and liver injury (Mizushima et al., 2002; Perlmutter, 2002), and autophagy is implicated in the execution of cell death (Xue et al., 1999; Bursch, 2001). However, the high level of autophagosome formation does not necessarily reflect enhanced protein degradation because the formation of autophagosomes is increased in Danon cardiomyopathy, which is characterized by defective lysosomal degradation (Nishino et al., 2000; Tanaka et al., 2000). Thus, it is not clear whether increased levels of autophagosome formation reflect the activation or defective protein degradation.

Although autophagy has been extensively studied, little was known about its molecular mechanism until the recent discovery of *ATG* genes in budding yeast (Tsukada and Ohsumi, 1993). Of the many *ATG* genes, seven uniquely compose two ubiquitin-like conjugation systems: ATG12 and ATG8 conjugation systems (Mizushima et al., 1998; Ichimura et al., 2000; Ohsumi, 2001). The ubiquitin-like protein Atg12p covalently attaches to Atg5p in a reaction similar to ubiquitination. In this process, Atg12p is activated by an E1-like enzyme, Atg7p (Tanida et al., 1999), and transferred to an E2-like enzyme, Atg10p (Shintani et al., 1999), and then finally conjugates to Atg5p. Atg8p, another ubiquitin-like protein, is unique among other ubiquitin-like molecules, as it conjugates to phosphatidyl-ethanolamine (Ichimura et al., 2000). Atg8p is activated by Atg7p, which is common to the Atg12 conjugation system, and is transferred to Atg3p, an E2-like enzyme (Ichimura et al., 2000). In mammals, there exist at least three Atg8 homologues that can all be activated by Atg7 (Tanida et al., 2001), GATE-16, GABARAP, and LC3 (Ohsumi, 2001), and they localize to the autophagosome (Kabeya et al., 2000, 2004).

Here, we generated conditional knockout mice of *Atg7* and analyzed the roles of autophagy in neonates and adult liver. Autophagosome formation and starvation-induced degradation of proteins and organelles was impaired in *Atg7*-deficient mice and adult livers. We also found an important role for autophagy in constitutive turnover of cytoplasmic components, and its loss resulted in accumulation of abnormal organelles and ubiquitinated proteins. Our results suggest that autophagy is important for clearance of ubiquitin-positive aggregates.

Results

Generation of *Atg7* conditional knockout mice

To investigate the physiological roles of autophagy in mammals, we generated *Atg7* conditional knockout mice. Mouse *Atg7* gene is encoded by 17 exons that span 216-kb long genomic DNA. The active site cysteine residue essential for activation of the substrates is encoded by exon 14 and the targeting vector is designed to conditionally disrupt this exon by Cre-*loxP* technology. The targeted exon 14 was modified so that it could express Atg7 even in the presence of neo-resistant gene cassette in intron 14 (Fig. 1 A). Mice homozygous for the $Atg7^{Flox}$ allele (referred to as $Atg7^{F/F}$ mice), which were expected to express intact Atg7, were born healthy and fertile without any noticeable pathological phenotypes. Fig. 1 B shows Southern blots of mice with the indicated genotypes. Immunoblot analysis revealed the presence of Atg7 protein in $Atg7^{F/F}$ mouse embryonic fibroblasts (MEFs; Fig. 1 C), suggesting that Atg7 is efficiently expressed from the $Atg7^{Flox}$ allele.

The phenotype of *Atg7*-deficient mice

To examine the *Atg7*-deficient phenotype, we bred $Atg7^{F/F}$ mice with a line of transgenic mice that express the Cre recombinase under the control of the Zp3 promoter in the oocyte (Lewandoski et al., 1997). The heterozygous mice (referred to as $Atg7^{+/-}$) were obtained from female $Atg7^{F/+}$:Zp3 mice. $Atg7^{+/-}$ mice were born healthy and fertile without any noticeable pathological phenotypes for 1 yr. The $Atg7^{-/-}$ mice, obtained by breeding $Atg7^{+/-}$ mice, were born at Mendelian frequency (+/+: +/−: −/− = 21: 38: 19). The results of PCR genotyping are shown in Fig. 2 A. Neither Atg7 mRNA nor protein was detected in the homozygous mice (Fig. 2, B and C). We also tested the loss of Atg7 activity by examining the ATG conjugation systems in the neonate liver. A 56-kD protein, equivalent to Atg5–Atg12 conjugate, was detected by Atg5 antibody in the control $Atg7^{+/-}$ but not $Atg7^{-/-}$ liver (Fig. 2 C). In contrast, free Atg5 of 30 kD, which was faintly observed in the $Atg7^{+/-}$ liver, increased in $Atg7^{-/-}$ liver (Fig. 2 C). Mammalian Atg8p homologue LC3 has two forms (i.e., LC3-I and LC3-II; Kabeya et al., 2000). It is generally accepted that LC3-I is the free mature form whereas LC3-II is the lipidated form, in analogy to yeast Atg8p (Ichimura et al., 2000; Kabeya et al., 2000). Both forms were detected in $Atg7^{+/-}$ liver whereas only the LC3-I form was detected and increased in $Atg7^{-/-}$ liver (Fig. 2 C). When crossed with GFP-LC3 transgenic mice (Mizushima et al., 2004), the punctate structures representing autophagosomes were detected in $Atg7^{+/-}$ but not in $Atg7^{-/-}$ heart (Fig. 2, D and E). These results indicate that *Atg7* is essential for ATG conjugation systems and autophagosome formation in mice.

Although homozygous mice seemed normal at birth (Fig. 2 F) and had no apparent developmental defect by histological analyses (Fig. S1, available at http://www.jcb.org/cgi/content/full/jcb.200412022/DC1), the mean body weight of $Atg7^{-/-}$ mice (0.983 ± 0.0763 g, ± SD, $n = 9$) was significantly lower than that of wild-type and heterozygote mice (1.20 ± 0.116 g, $n = 29$; $P < 0.01$), and $Atg7^{-/-}$ mice died within 1 d after birth ($n = 19$). We considered that $Atg7^{-/-}$ mice could survive in utero by virtue of the nutrients supplied through the placenta but could not survive when the supply terminates after birth, as recently reported (Kuma et al., 2004). We tested the survival time of $Atg7^{-/-}$ neonates under starvation condition after caesarean delivery. Wild-type and heterozygous mice died at 21.7 ± 3.3 h after birth, whereas $Atg7^{-/-}$ mice died at 13 ± 2.0 h ($P < 0.01$; Fig. 2 G). To further test whether the cause of earlier death correlates with lower nutrient supply, we measured amino acid concentrations in plasma at 10 h after caesarean delivery. Essential and branched-chain amino acid concentrations in the sera of $Atg7^{-/-}$ mice were lower than those of wild-type mice (essential amino acids: 1.536 ± 0.087 vs. 1.291 ± 0.166 mmol/L, $P < 0.05$; branched-chain amino acids: 0.375 ± 0.038 vs. 0.268 ± 0.015 mmol/L, $P < 0.01$, respectively). The same

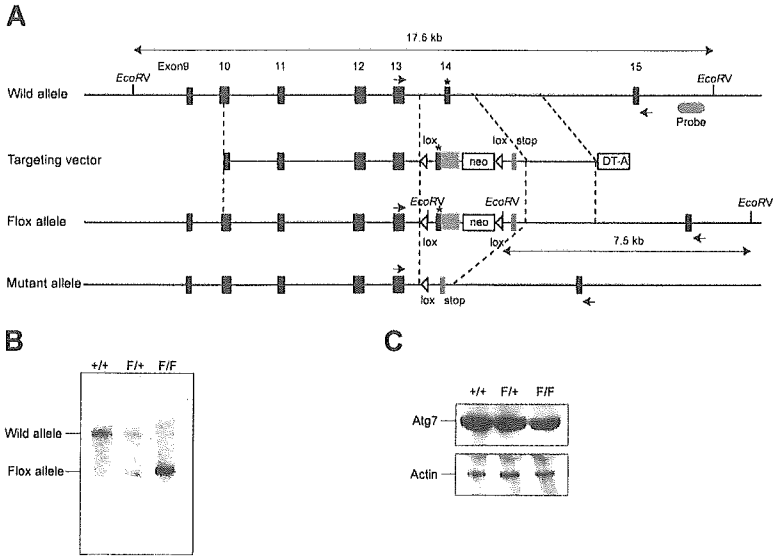

Figure 1. **Generation of *Atg7*$^{F/F}$ mice.** (A) Schematic representation of the targeting vector and the targeted allele of *Atg7* gene. The coding exons numbered in accordance with the initiation site as exon 1 are depicted by black boxes. Green and red boxes indicate *Atg7* cDNA fragment (aa 1786–2097) and *Atg7* cDNA fragment (aa 1669–1698) with stop codon, respectively. The open triangles denote *loxP* sequence. A probe for Southern blot analysis is shown as a gray ellipse. Arrows indicate the positions of PCR primers. The asterisk denotes the essential cysteine residue on exon 14. EcoRV, EcoRV sites; neo, neomycin-resistant gene cassette; DT-A, diphtheria toxin gene. (B) Southern blot analysis of genomic DNAs extracted from mice tails. Wild-type and Flox alleles are detected as 17.5- and 7.5-kb bands, respectively. (C) Immunoblot of Atg7 in MEFs. The lysates of MEFs of indicated genotypes were immunoblotted with Atg7 and actin.

results were also obtained using MEF cells from *Atg7*$^{-/-}$ mice (unpublished data). Together, these results indicate that *Atg7* is crucial for the recycling of amino acids in cells and survival of newborn mice under starvation condition.

Starvation response in adult mice liver

To delete *Atg7* gene in the adult mice, we bred the *Atg7*$^{F/F}$ mice with Mx1-Cre transgenic mice that express the Cre recombinase in response to interferon γ or its chemical inducer, polyinosinic acid–polycytidylic acid (pIpC). The Mx1-Cre transgenic mice can excise Flox allele completely in the liver and spleen and partially in the kidney and heart (Kuhn et al., 1995). Intraperitoneal injections of pIpC resulted in effective recombination of the *Atg7*^{Flox} allele in the liver and spleen (Fig. S2, available at http://www.jcb.org/cgi/content/full/jcb.200412022/DC1; and not depicted). No Atg7 transcript, protein, and activity were detected, similar to *Atg7*$^{-/-}$ mice (Fig. S2). Next, we tested the autophagosome formation under fasting condition. 1-d fasting resulted in induction of typical autophagosomes in control *Atg7*$^{F/+}$:Mx1 mice (Fig. 3, A–D and I). In contrast, no such induction of autophagosome formation was noted in the liver of fasted *Atg7*$^{F/F}$:Mx1 mice (Fig. 3, E, F, and I). Although some autophagosome-like structures were occasionally observed both in fed and fasted mutant mice livers (Fig. 3, G and H), they

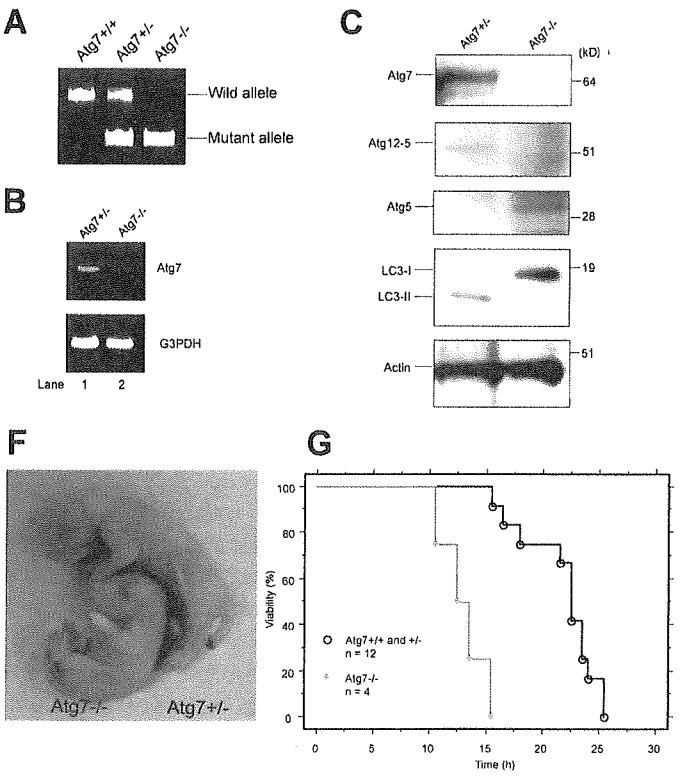

Figure 2. **The phenotypes of *Atg7*-deficient mice.** (A) PCR analysis of genomic DNA extracted from wild-type, *Atg7*$^{+/-}$, and *Atg7*$^{-/-}$ mice tail. The amplified fragments derived from wild and mutant alleles are indicated. (B) Expression of Atg7 transcript. Atg7 transcript was detected by RT-PCR analysis. The region amplified was between exons 12 and 13. G3PDH cDNA was amplified as an internal control. (C) ATG conjugation systems in *Atg7*$^{-/-}$ mice liver. The liver homogenate was centrifuged at 800 *g* for 10 min and the postnuclear supernatant (PNS) was immunoblotted with antibodies against Atg7, Atg5, LC3, and actin as a loading control. The bottom panel of Atg5 blotting is the long exposure of the top panel to detect free Atg5. Data shown are representative of three separate experiments. (D and E) Deficiency of autophagosome formation in *Atg7*$^{-/-}$ heart. *Atg7*$^{+/-}$ (D) and *Atg7*$^{-/-}$ (E) mice expressing GFP-LC3 were obtained by caesarean delivery and analyzed by fluorescence microscopy. Representative results obtained from each neonatal heart at 3 h after caesarean delivery. (F) Morphology of *Atg7*$^{+/-}$ and *Atg7*$^{-/-}$ mice. (G) Kaplan-Meier curves of survival of newborn mice. Control and *Atg7*$^{-/-}$ mice were delivered by caesarean section, and their survival was followed up to 26 h.

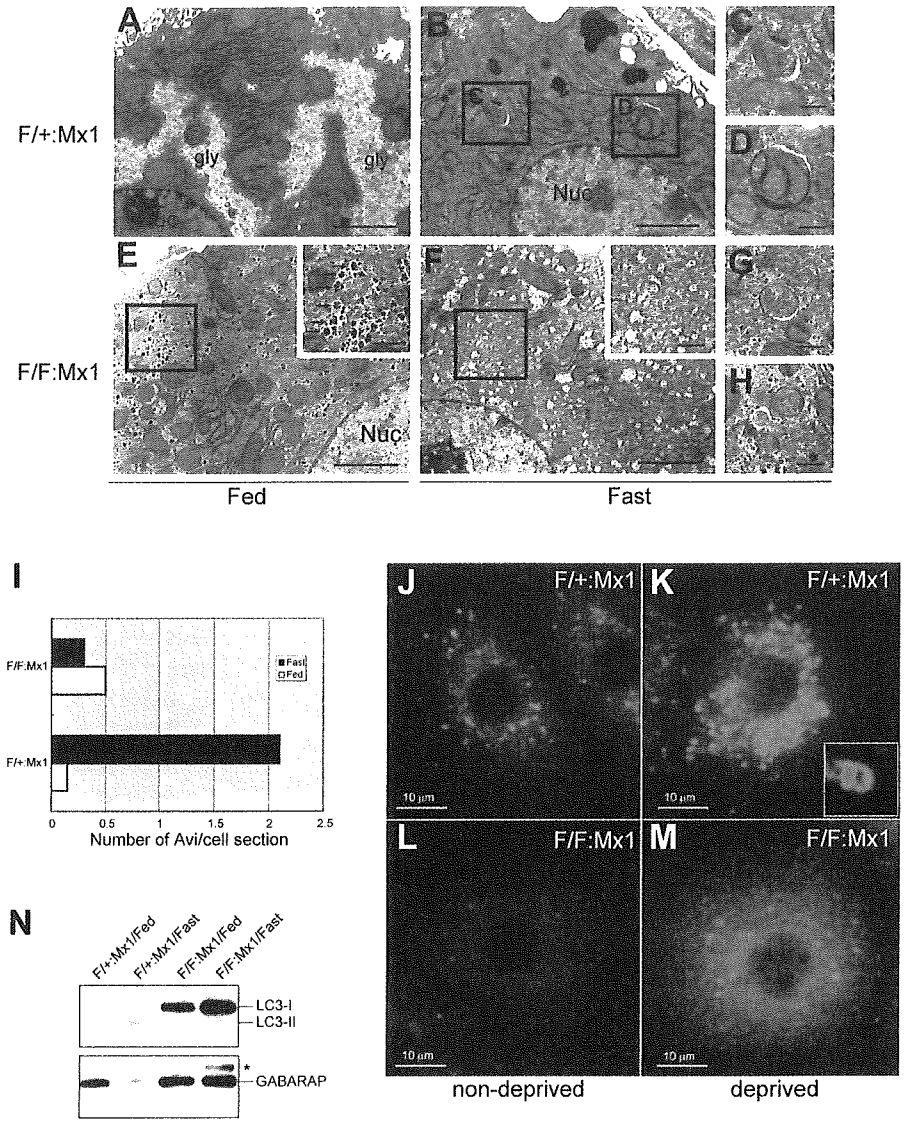

Figure 3. **Impaired autophagosome formation in *Atg7*-deficient liver.** (A–H) Electron micrographs of liver from $Atg7^{F/+}$:Mx1 (A–D) and $Atg7^{F/F}$:Mx1 (E–H) mice fed ad libitum (A and E) or fasted for 1 d (B and F). (C and D) Early stages of autophagic vacuoles observed in B are highlighted. (E and F) Autophagosome was not induced in mutant hepatocytes upon fasting. Insets show higher magnification views of glycogen granules. (G and H) Occasionally observed autophagosome-like structures in mutant hepatocytes. Bars: (A, B, E, and F) 5 μm; (C, D, G, and H) 0.5 μm. (I) Number of autophagosomes per hepatocyte (n = 20) in each genotype was counted and their averages are shown. (J–M) Immunofluorescent analysis of LC3 in primary cultured hepatocytes. Hepatocytes isolated from $Atg7^{F/+}$:Mx1 (J and K) and $Atg7^{F/F}$:Mx1 mice (L and M) were cultured in Williams' E (J and L) or Hanks' solution (K and M). Inset highlights the cup-like structure of LC3 observed in K. (N) Immunoblot analysis of Atg8 homologues in the liver. $Atg7^{F/+}$:Mx1 (lanes 1 and 2) and $Atg7^{F/F}$:Mx1 mice (lanes 3 and 4) were fed ad libitum (lanes 1 and 3) or fasted for 1 d (lanes 2 and 4), and then PNS fractions of liver were analyzed by immunoblotting with anti-LC3, GABARAP, GATE-16, and actin antibodies. Asterisk denotes a nonspecific band. Data shown are representative of three separate experiments.

tended to be smaller than those observed in fasted control liver and hardly contained large cytoplasmic organelles (compare with Fig. 3, C and D). The number of autophagosomes per hepatocyte was counted and the mean values are shown in Fig. 3 I. The mutant hepatocytes lacked typical glycogen area, in contrast to the fed hepatocytes (Fig. 3, A and E); however, well-developed glycogen granules (α granules) were observed between numerous smooth endoplasmic reticula (Fig. 3 E, inset). Immunofluorescent analysis also revealed the presence of many cup-shaped and ringlike structures representing autophagosomes in the control hepatocytes (Fig. 3, J and K). Although several LC3-positive dots were observed in the mutant hepatocytes, they were not induced in response to starvation and did not form cup-shaped and ringlike structures (Fig. 3, L and M).

Next, we examined the fasting response of LC3 and other homologues, GABARAP and GATE-16, by immunoblotting (Fig. 3 N). LC3 is known to be up-regulated and recruited to the autophagosome upon starvation and degraded in the lysosomes (Kabeya et al., 2000). Fasting slightly increased the modification of LC3 in heterozygous liver. In the mutant liver, no modification of LC3 was noted and LC3-I increased in response to fasting. These results suggest that LC3 is up-regulated, but its modification and degradation are impaired in mutant mice. The level of GABARAP did not change upon fasting in the mutant liver, whereas it decreased in the heterozygous liver, suggesting that GABARAP is not up-regulated but its degradation after modification is impaired in mutant liver. Although GATE-16 was hardly detected in the heterozygous liver under both fed and fasting conditions, it was clearly detected

and increased upon fasting in the mutant liver. These results suggest that GATE-16 may be constitutively degraded even at fed condition in heterozygous mice and up-regulated in response to fasting under defective *Atg7*. The levels of all LC3 homologues were elevated even at fed condition in the mutant liver, suggesting their marked stabilization in autophagy-deficient condition. However, the possibility that their transcriptions are up-regulated at basal level due to *Atg7* deficiency cannot be excluded. We sought to determine their localizations in the cells. However, our antibodies for these molecules were not applicable for immunofluorescent analyses, and those localizations remain to be clarified. In conclusion, all Atg8 homologues respond to fasting, although in a different manner, and their levels are affected by the absence of Atg7.

Atg7 is indispensable for fasting-induced degradation of cytosolic proteins and organelles in the mouse liver

Given that autophagosome formation was impaired in *Atg7*-deficient liver, we next examined its effects on the bulk degradation of proteins and organelles under fasting condition. After 1-d fasting in control $Atg7^{F/+}$:Mx1 and mutant $Atg7^{F/F}$:Mx1 mice, the liver was dissected and the amount of total protein per whole liver was measured. The amount of total liver proteins decreased to ~66% by 1-d fasting in the control liver (Fig. 4 A). In contrast, fasting did not significantly decrease the amount of total liver proteins in the mutant liver. Moreover, the amount of total proteins in the mutant liver was 1.5-fold that of control. These results indicate that the decrease of total proteins is dependent on Atg7 and autophagosome formation.

We also examined whether or not fasting causes the degradation of cellular organelles such as mitochondria in the livers of mice. To quantify the amount of the mitochondria, we first measured the activity of mitochondrial enzyme succinate dehydrogenase (SDH) in total liver extracts. In the control livers, fasting was associated with a significant decrease of SDH activity, and the reduction was proportional with the decrease in the amount of total protein (Fig. 4 B). In contrast, fasting was not associated with any change in SDH activity in the mutant livers. Similar to total protein, the basal SDH activity in mutant liver was significantly higher than in control. The effect of fasting on the amount of the mitochondria was also assessed by immunoblot analysis of mitochondrial protein cytochrome *c* (Fig. 4 C). When equal amounts of proteins were loaded, the level of cytochrome *c* was equivalent in the two genotypes at either fed or fasting conditions, suggesting that the ratio of mitochondria versus total protein is not altered by fasting in both genotypes. Considering that the total protein amounts decreased by fasting in the control liver (Fig. 4 A), these results suggest that the mitochondria and cytoplasmic proteins are proportionally degraded upon fasting in heterozygous mice. However, such degradation is impaired in *Atg7*-deficient liver because the levels of both proteins and mitochondria are unchanged and kept at a higher level.

Next, we investigated the effect of autophagy deficiency on protein turnover. To quantify the turnover of long-lived protein, after each control and mutant hepatocytes had been labeled with [^{14}C]leucine for 24 h and chased for 2 h, the release of TCA-soluble [^{14}C]leucine was measured for 4 h. In control hepatocytes, nutrient deprivation significantly induced protein degradation, and such degradation was suppressed by the addition of lysosomal inhibitors such as monomethylamine and E64d and pepstatin (Fig. 4 D). The induced degradation was still observed in the presence of proteasome inhibitor epoxomicin, suggesting that such protein degradation is mediated in the lysosomal pathway rather than the proteasome (Fig. 4 D). In the mutant hepatocytes, degradation of long-lived protein was not induced by nutrient deprivation (Fig. 4 D), indicating that autophagy is the main route for lysosomal degradation under starvation condition. Consistent with these results, amino acid concentrations in starved mutant hepatocytes were lower than in control hepatocytes (unpublished data). Intriguingly, although lysosomal inhibitors inhibited protein degradation even

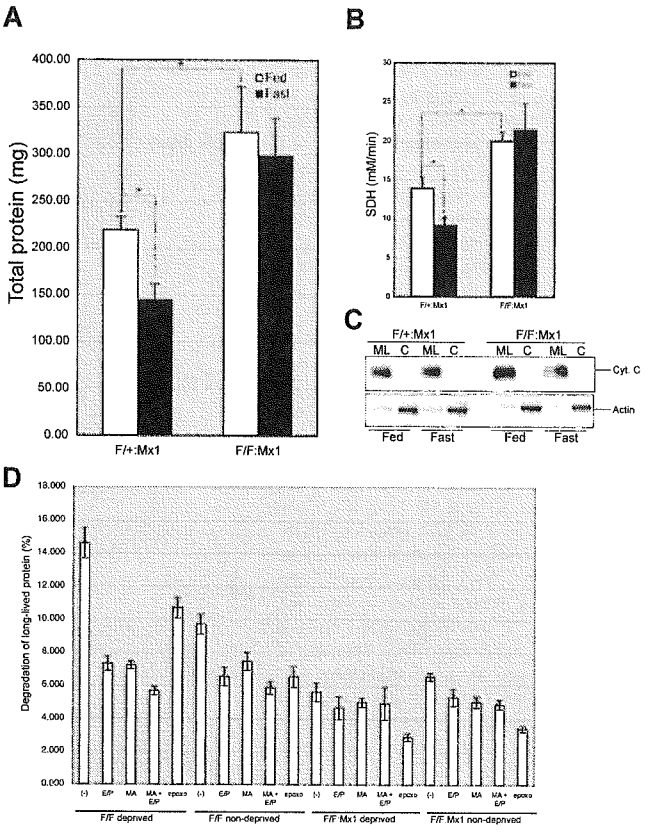

Figure 4. **Fasting response of *Atg7*-deficient liver.** (A and B) Livers from $Atg7^{F/+}$:Mx1 and $Atg7^{F/F}$:Mx1 mice fed ad libitum (Fed) or fasted for 1 d (Fast) at 20 d after pIpC injection were dissected, and the amount of total protein (A) and SDH activity (B) per liver were measured. Data are mean ± SD values of five mice in each group; *, $P < 0.01$. (C) Cytochrome *c* levels in the cytosolic and mitochondria/lysosomal fractions of the liver at 20 d after injection. Equal amount of PNS fractions were centrifuged at 8,000 *g* for 10 min and the pellets were used as the mitochondrial/lysosomal fraction (ML). The supernatants were further centrifuged at 100,000 *g* for 1 h and the supernatant was used as the cytosolic fraction (C). Actin was blotted as control. Data shown are representative of two separate experiments. (D) Turnover of long-lived protein. Hepatocytes from $Atg7^{F/+}$:Mx1 and $Atg7^{F/F}$:Mx1 mice were isolated and labeled with [^{14}C]leucine for 24 h, and degradation of long-lived protein in deprived or nondeprived condition was measured. Monomethylamine (MA) and/or E64d and pepstatin (E/P) or epoxomicin (epoxo) was added as indicated. Data are the mean ± SD of triplicate experiments.

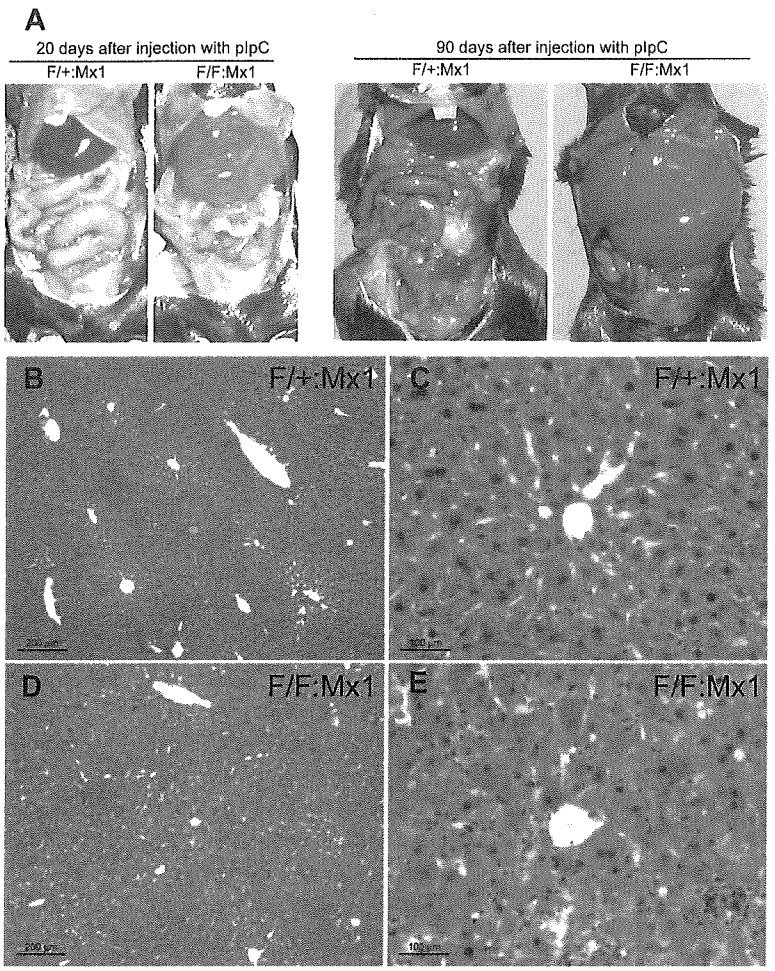

Figure 5. ***Atg7* deficiency in the liver causes hepatomegaly and hepatic cell swelling.** (A) The gross anatomical views of representative mice at the indicated day after pIpC injection. (B–E) Histology of representative livers with *Atg7* deficiency. Hematoxylin and eosin staining of $Atg7^{F/+}$:Mx1 (B and C) and $Atg7^{F/F}$:Mx1 (D and E) liver at 90 d after pIpC injection.

at nondeprived condition in the control hepatocytes, such inhibition was not significant in the mutant hepatocytes (Fig. 4 D), indicating that significant amounts of proteins are constitutively degraded in the lysosome via autophagic pathway. Together, these results suggest that autophagy plays a significant role in turnover of long-lived protein.

Loss of *Atg7* in the liver leads to hepatomegaly and accumulation of abnormal organelles in hepatic cells

We further chased the phenotypes of the mutant mice for up to 90 d after pIpC injection. Gross anatomy revealed severe enlargement of the liver, filling up most of the abdominal cavity (Fig. 5 A). Other major organs were normal histologically (Fig. S3, available at http://www.jcb.org/cgi/content/full/jcb.200412022/DC1). The mean liver weights of control and mutant mice at 90 d after pIpC injection were 1.39 ± 0.24 and 6.10 ± 2.06 g, respectively (n = 5 each). Histological analysis revealed disorganized hepatic lobules and cell swelling in the mutant liver (Fig. 5, D and E). No hepatocellular proliferation or regeneration was detected (unpublished data). Vacuolated hepatic cells were occasionally observed and those were associated with hepatic cell death, which is consistent with the leakage of alkaline phosphatase, aspartate aminotransferase, and alanine aminotransferase in the mutant mice sera (Fig. S4, available at http://www.jcb.org/cgi/content/full/jcb.200412022/DC1).

Although most hepatocytes were still alive in the mutant liver, ultrastructural analysis revealed the appearance of aberrant concentric membranous structures (Fig. 6, A and B), which were also observed as early as 20 d after pIpC-injected liver (not depicted). These structures surrounded various cytoplasmic constituents such as mitochondria, lipid droplets, and vesicular structures (Fig. 6 A). Their membranous elements were continuous with the rough ER (Fig. 6 B, arrowheads), and the corresponding structures were positive for calreticulin, an ER protein marker (not depicted), indicating that these structures originated from the rough ER. Accumulation of peroxisomes (Fig. 6 C) and deformed mitochondria (Fig. 6, C and D) was also observed in the mutant liver. These results suggest the important role of autophagy in turnover of organelles, and its defect results in accumulation of abnormal organelles.

Formation of ubiquitin-positive inclusions in *Atg7*-deficient hepatocytes

Autophagy has been implicated in not only organelle turnover but also in elimination of protein aggregates (Kopito, 2000). Protein aggregates are often ubiquitinated. In the next step, we immunostained the liver with an ubiquitin antibody to examine the presence of such aggregates. Several ubiquitin-positive par-

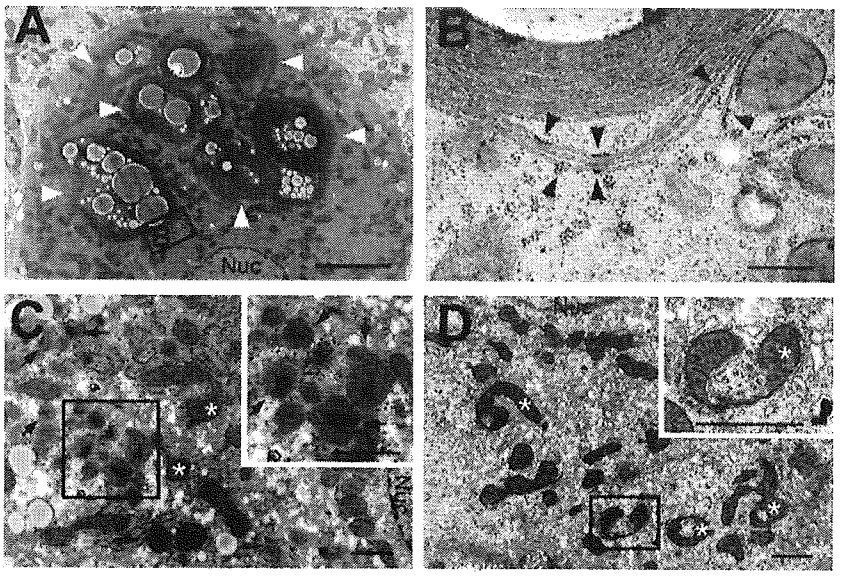

Figure 6. **Electron micrographs of hepatic cells with *Atg7* deficiency.** (A and B) Note the presence of concentric membranous structures in the mutant cells (arrowheads). Higher magnification view (B) shows the membranous elements are continuous with the rough ER (arrowheads). (C and D) The mutant cells contained a high number of peroxisomes (arrows) and deformed mitochondria (asterisks). Insets show higher magnification views. Nuc, nucleus. Bars: (A) 5 μm; (B) 0.5 μm; (C and D) 1 μm.

ticles of various sizes were detected in the $Atg7^{F/F}$:Mx1 but not in $Atg7^{F/+}$:Mx1 hepatic cells at both 10 and 90 d after pIpC injection (Fig. 7, A and B; and Fig. S5, available at http://www.jcb.org/cgi/content/full/jcb.200412022/DC1). The immunoblots of the liver lysates revealed the accumulation of high-molecular mass polyubiquitinated proteins in the mutant liver (Fig. 7 G and Fig. S5), suggesting that the ubiquitin particles are aggregates of polyubiquitinated proteins. To further determine the localization of ubiquitin-positive dots, analysis of immunoelectron micrographs was performed. Numerous particles of colloidal gold, indicative of ubiquitin, were detected on lipid dropletlike structures, membranous structures, and amorphous substances in the cytoplasm (Fig. 7, C–F). Such signals were not observed in the wild-type liver (unpublished data).

The accumulation of ubiquitin-positive inclusions in the cytoplasm prompted us to examine the effect of autophagy deficiency on proteasome function. Immunoblots of proteasome subunits (p112/Rpn2, Mss1/Rpt1, and α5) showed that their relative amounts were not affected in the mutant liver (Fig. 7 G). Furthermore, the activities of the proteasome, measured by Suc-LLVY-MCA as substrate, were also comparable between wild-type and mutant livers (unpublished data). These results indicate the accumulation of ubiquitin-positive aggregates in autophagy-deficient hepatocytes despite the apparently normal proteasome function.

Discussion

Autophagy is a bulk protein degradation pathway, which is conserved in eukaryotes, essential for the survival of unicellular organisms under nutrient-poor condition and for cellular remodeling of multicellular organisms (Mizushima et al., 2002; Levine and Klionsky, 2004). In the present study, we generated conditional knockout mice of *Atg7* gene, which is an essential gene for autophagy in budding yeast, and analyzed its roles in mice.

In mammals, *Atg7* was indeed essential for ATG12 conjugation, LC3 modification systems, and autophagosome formation (Fig. 2, Fig. 3, and Fig. S2). Immunofluorescent analyses revealed that LC3-positive dots appeared but did not form cup-shaped and ringlike structures in $Atg7^{F/F}$:Mx1 livers (Fig. 3). The LC3-I form is usually present at the S100 fraction and the LC3-II form at the P100 fraction (Kabeya et al., 2000). In the mutant liver, LC3-I was present in both S100 and P100 fractions (unpublished data), suggesting that the LC3-positive dots in the mutant hepatocytes are indeed the LC3-I form. These results suggest that LC3 may be recruited to the dot structures independent of the modification (Fig. 3). In mammals, LC3 has at least two homologues, GABARAP and GATE-16, which share common biochemical characteristics (Tanida et al., 2001) and localize to autophagosome in response to fasting (Kabeya et al., 2004). Indeed, the modification and levels of these molecules under fasting condition were affected in the mutant liver (Fig. 3 N). However, these LC3 homologues have been identified in a different biological pathway and may have diverse functions (Ohsumi, 2001). Thus, how their functions and localizations are affected in *Atg7*-deficient cells remains to be clarified.

Although $Atg7^{-/-}$ mice were born at Mendelian ratio, and the major organs were almost normal histologically (Fig. S1), they had reduced body weight and died within 1 d after birth. $Atg7^{-/-}$ mice had lower amino acid level and died earlier compared with wild type under nonsuckling condition after caesarean delivery (Fig. 2 G), suggesting that *Atg7* is important for survival during the early neonatal starvation period, similar to recently reported $Atg5^{-/-}$ mice phenotypes (Kuma et al., 2004). However, because suckling $Atg7^{-/-}$ mice also died within 1 d after birth (unpublished data), the cause of death may not be only due to low level of amino acids. The reason for the reduced body size is also unclear and may be related to placental function or due to inefficient reutilization of nutrients during embryogenesis. It is of note that a lower level of autophagy occurs during embryogenesis (Mizushima et al., 2004) even when nutrients are supplied from the placenta. Furthermore, *Atg7* null mice possess several ubiquitin-positive inclusions in some

organs at the time of birth (unpublished data). This phenotype might be related to the earlier death of mutant. Further analysis of $Atg7^{-/-}$ mice is required to unravel the roles of autophagy, and such analysis is currently under way by breeding the $Atg7^{F/F}$ mice with several Cre-transgenic mice.

Starvation-induced autophagosomes appeared to sequester the cytoplasm randomly (Fig. 3). Consistent with this notion, the amount of mitochondria decreased in proportion with reduction in the amount of total protein (Fig. 4, A–C). These results suggest that mitochondria are degraded nonselectively under fasting condition. In *Atg7*-deficient liver, no autophagosome formation was noted and the degradation of proteins and organelles under fasting condition was largely impaired. These results suggest that the rapid reduction of proteins and organelles upon fasting is dependent on *Atg7* and autophagosome formation.

Although autophagy can be induced by starvation, this pathway may take place even at feeding condition at basal level. This constitutive pathway may be important for turnover of organelles and cytoplasmic proteins. Indeed, the degradation of long-lived protein was inhibited in mutant hepatocytes irrespective of nutrient deprivation (Fig. 4 D), and multiple abnormalities of organelles (e.g., the presence of concentric membranous structure and accumulation of deformed mitochondria) were observed in *Atg7*-deficient hepatocytes (Fig. 6). Unexpectedly, the morphologically abnormal mitochondria appear to retain their function, as judged by the normal membrane potentials and the absence of cytochrome *c* leakage in the cytosol (unpublished data). In contrast to starvation-induced autophagy, whether or not constitutive autophagy eliminates abnormal and excess organelles in a degree of selectivity remains to be clarified.

Beclin 1, a human homologue of *ATG6/VPS30* essential for autophagy in yeast, was recently identified as a tumor suppressor gene, and autophagy has been implicated in the regulation of cellular proliferation (Liang et al., 1999). Indeed, heterozygous disruption of mouse *Beclin 1* led to enhanced tumorigenesis (Qu et al., 2003; Yue et al., 2003). *Atg7* deficiency led to hepatomegaly (Fig. 5 A), suggesting that cell proliferation or malignant transformation might be induced in the *Atg7*-deficient cells. However, neither tumorigenesis nor enhanced cell proliferation was detected as tested by BrdU incorporation at 90 d after pIpC injection in the mutant liver compared with control mice (unpublished data). The hepatomegaly observed in the mutant mice was likely due to increased cellular volume rather than cell number, which is also supported by the swollen appearance of hepatocytes (Fig. 5, D and E).

In *Atg7*-deficient liver, we detected numerous ubiquitin-positive particles indicative of protein aggregates (Fig. 7 and Fig. S5). It has been reported that proteasome inhibition leads to aggregate formation. Conversely, the formation of protein aggregates inhibits the proteasome (Bence et al., 2001), resulting in a malignant cycle of aggregate formation and proteasome inhibition. In the mutant liver, failure of the proteasome was postulated; however, no impairment of proteasome function, in terms of its expression or peptidase activities, was noted (Fig. 7 G and not depicted). Our results suggest that the ubiquitinated proteins eventually aggregate even in the presence of functional proteasomes. Considering that such ubiquitinated aggregates must be difficult to unfold, and proteasomes need to unfold their substrate before degradation (Baumeister et al., 1998), it is likely that elimination of ubiquitin-positive aggregates in the cells is largely dependent on the autophagic process. Protein ubiquitination may also occur after protein aggregation. In either case, we propose the possibility that protein ubiquitination may serve as a signal to the autophagic process in addition to the proteasomes pathway. In this context, it is worth noting that sperm mitochondria are known to be ubiquitinated before degradation during fertilization (Sutovsky et al., 1999). It is now well established that ubiquitin regulates not only proteasomal degradation, but also lysosomal degradation. Thus, it is conceivable that ubiquitin could also regulate the autophagic pathway.

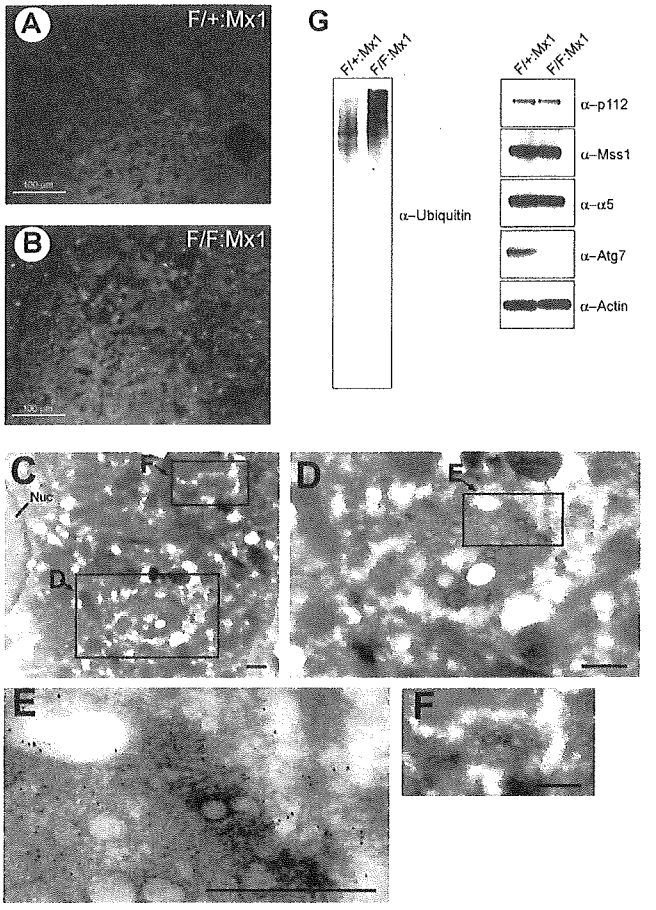

Figure 7. **Accumulation of ubiquitin-positive aggregates in *Atg7*-deficient liver.** (A and B) Immunofluorescent detection of ubiquitin in the $Atg7^{f/+}$:Mx1 (A) and $Atg7^{f/f}$:Mx1 (B) liver. (C–F) Immunoelectron micrographs of ubiquitin in a representative mutant liver. The high-magnification view shows ubiquitin particles near the lipid dropletlike structure (D–F). Bars, 0.5 μm. (G) Immunoblot analysis of the liver. PNS fractions of the liver at 90 d after injection were immunoblotted with the indicated antibodies. Data shown are representative of three separate experiments.

A growing number of disease-associated proteins have been found to accumulate in aggresome, including huntingtin, parkin, α-synuclein, and peripheral myelin protein 22 (Notterpek et al., 1999; Ciechanover and Brundin, 2003). The aggregation of these proteins is thought to be involved in the pathogenesis of Huntington's disease, Parkinson's disease, and peripheral neu-

ropathies, respectively. Enhanced autophagosome formation is prevalent in most of these diseases (Mizushima et al., 2002), and autophagy has also been considered as a caspase-independent cell death pathway (Xue et al., 1999; Bursch, 2001). Our *Atg7* mutant mice should be useful for examining the role of autophagy in the cell death pathway or in a cellular defense mechanism in the pathogenesis of these diseases.

Materials and methods

Generation of $Atg7^{f/F}$ mice

The targeting vector was constructed by insertion of a *loxP* sequences within introns 13 and 14 of *Atg7* gene. Exon 14 was fused to a cDNA fragment encoded by exons 15, 16, and 17 (aa 1786–2097) and polyA signal sequence was added after the stop codon. Neo resistant gene cassette (*mc1-neo-pA*) was ligated behind the polyA signal sequence followed by the second *loxP* sequence, splicing acceptor site, and exon 14 with stop codon preceding the active site. We electroporated the targeting vector into mouse TT2 ES cells, selected with 200 μg/ml G418 (GIBCO BRL), and then screened for homologous recombinants by PCR and Southern blot analyses. PCR primers were as follows: 5′-TGGCTGCTACTTCTGCAATGATGT-3′, 5′-GAAGGGACTGGCTGCTATTGGGCGAAGTGC-3′, and 5′-TTAGCACAGGGAACAGCGCTCATGG-3′. Southern blot analysis was performed by digestion of genomic DNA with EcoRV and hybridization with the probe shown in Fig. 1 A. Genotyping of mice by PCR was performed using the following two primers: 5′-TGGCTGCTACTTCTGCAATGATGT-3′ and 5′-CAGGACAGAGACCATCAGCTCCAC-3′. Progeny containing the $Atg7^{Flox}$ allele were bred with *Zp3*-Cre and *Mx1*-Cre transgenic mice to produce $Atg7^{-/-}$ and $Atg7^{f/F}$:Mx1 mice, respectively. With regard to $Atg7^{f/F}$:Mx1 mice, Cre expression in the liver was induced by i.p. injection of pIpC (Sigma-Aldrich). 300 μl pIpC solution (1 mg/ml in water) was injected three times at 48-h intervals. Mice were housed in specific pathogen-free facilities, and the experimental protocol was approved by the Ethics Review Committee for Animal Experimentation of the Tokyo Metropolitan Institute of Medical Science.

RT-PCR analysis

cDNA was synthesized from 5 μg of DNase I–treated total RNA using the SuperScript First-Strand Synthesis System (GIBCO BRL) and oligo $(dT)_{12\text{-}18}$ primers. Specific primers for each gene were as follows: 5′-ATGCCAGGACACCCTGTGAACTTC-3′ and 5′-ACATCATTGCAGAAGTAGCAGCCA-3′ for Atg7, and 5′-GAGCTGAACGGGAAGCTCAC-3′ and 5′-ACCACCCTGTTGCTGTAGC-3′ for G3PDH.

Immunoblot analysis

The fractions were immunoblotted as described previously (Komatsu et al., 2001). The antibodies for Atg7 (Tanida et al., 1999) and Atg5 (Mizushima et al., 2001) were described previously. The antibodies for ubiquitin (DakoCytomation) and actin (MAB1501R; Chemicon International, Inc.) were purchased. The antibodies against LC3, GABARAP, and GATE-16 were raised in rabbits using their specific peptides as antigens. The antibodies against p112, Mss1, and α5 were provided by K.B. Hendil (August Krogh Institute, University of Copenhagen, Copenhagen, Denmark).

Caesarean delivery and measurement of amino acids

Newborns were delivered by caesarean section at 19.0 d postcoitus and placed in a humidified, thermostat-controlled chamber (30°C). Plasma was fixed in 3% sulphosalicylic acid. Amino acids in the supernatant from plasma samples were measured by an amino acid analyzer (L8500A; Hitachi).

Protein degradation assay

The assay was performed essentially as described previously (Gronostajski and Pardee, 1984). In brief, hepatocytes were plated at 5×10^4 cells/well in collagen-coated 24-well plates and cultured in Williams' E medium with 10% FCS (Williams' E/10% FCS) for 24 h. Cells were incubated with Williams' E/10% FCS containing 0.5 μCi/ml [^{14}C]leucine for 24 h to label long-lived proteins. Cells were washed with Williams' E/10% FCS containing 2 mM of unlabeled leucine and incubated with the medium for 2 h to allow degradation of short-lived proteins and minimize the incorporation of labeled leucine, which was released by proteolysis into protein. The cells were then washed with PBS and incubated at 37°C with Krebs-Ringer bicarbonate medium and Williams' E/10% FCS in the presence or absence of protease inhibitors (5 mM monomethylamine, 10 μg/ml E64d and pepstatin, or 5 μM epoxomicin). After 4 h, aliquots of the medium were taken and a one-tenth volume of 100% trichloroacetic acid was added to each aliquot. The mixtures were centrifuged at 12,000 *g* for 5 min, and the acid-soluble radioactivity was determined using a liquid scintillation counter. At the end of the experiment, the cultures were washed twice with PBS, and 1 ml of cold trichloroacetic acid was added to fix the cell proteins. The fixed cell monolayers were washed with trichloroacetic acid and dissolved in 1 ml of 1 N NaOH at 37°C. Radioactivity in an aliquot of 1 N NaOH was determined by liquid scintillation counting. The percentage of protein degradation was calculated according to published procedures (Gronostajski and Pardee, 1984).

Histological examination

Tissues were dissected, fixed in 4% PFA, paraffin embedded, and sectioned. Sections were stained by Meyer's hematoxylin and eosin. For immunohistochemical analysis, sections were blocked in 5% normal goat serum in PBS containing 0.2% Triton X-100, and then incubated with antiubiquitin antibody (1B3; MBL International Corporation) and Alexa 488–labeled secondary antibody (Molecular Probes). Apoptotic cells were detected by TUNEL assay using Apoptag kit (Intergen Company) as described previously (Tateishi et al., 2001). For GFP-LC3 observations, tissues were fixed with 4% PFA, and the cryosections were imaged with a conventional fluorescence microscope. For LC3 staining, hepatocytes were fixed and stained with anti-LC3 antibody as described previously (Kabeya et al., 2000). All fluorescence images were obtained using a fluorescence microscope (model Q550FV; Leica) equipped with cooled charge-coupled device camera (model CTR MIC; Leica). Pictures were taken using Qfluoro software (Leica).

EM and immunoelectron microscopy

Livers were fixed by cardiac perfusion using 0.1 M phosphate buffer containing 2% PFA and 2% glutaraldehyde for conventional EM. They were post-fixed with 1% OsO_4, embedded in Epon812, and sectioned. Immunoelectron microscopy was performed on cryothin sections as described previously (Waguri et al., 1995). In brief, livers were frozen in phosphate buffer with 2.3 M sucrose and 20% polyvinyl pyrrhoridon. Ultrathin sections were mounted on Formvar carbon-coated nickel grids, blocked with 1% BSA in PBS, and incubated with antiubiquitin antibody (1B3) and colloidal gold conjugated secondary antibody.

Other procedures

MEFs were prepared as described previously (Murata et al., 2001). Primary hepatocytes were prepared as described previously (Ueno et al., 1990). Cell starvation was conducted by incubating the cells in Hanks' balanced solution after three separate washes. The SDH activity was assayed as described previously (Ueno et al., 1990).

On line supplemental material

Fig. S1 shows the histological analyses of tissues from $Atg7^{+/-}$ and $Atg7^{-/-}$ mice at 1 d after birth. Fig. S2 shows the loss of Atg7 protein and activity in $Atg7^{f/f}$:Mx1 mouse liver. Fig. S3 shows the histological analyses of tissues from $Atg7^{f/+}$:Mx1 and $Atg7^{f/F}$:Mx1 mice. Fig. S4 shows the cell death in autophagy-deficient liver. Fig. S5 shows the accumulation of ubiquitin-positive inclusions at early stage of autophagy deficiency. Further comments on the data can be found in the legends. Online supplemental material is available at http://www.jcb.org/cgi/content/full/jcb.200412022/DC1.

We thank T. Kaneko, T. Kouno, and K. Tatsumi for technical assistance. We also thank F. Kaji for his help in EM study; A. Kuma for technical guidance in caesarean delivery; K. Tateishi and H. Uozaki for discussion of liver pathology; and T. Fujimura and K. Murayama for amino acid measurements.

This work was supported in part by Grants-in-Aid from the Ministry of Education, Culture, Sports, Science and Technology of Japan.

Submitted: 3 December 2004
Accepted: 22 March 2005

References

Baumeister, W., J. Walz, F. Zuhl, and E. Seemuller. 1998. The proteasome: paradigm of a self-compartmentalizing protease. *Cell.* 92:367–380.

Bence, N.F., R.M. Sampat, and R.R. Kopito. 2001. Impairment of the ubiquitin-proteasome system by protein aggregation. *Science.* 292:1552–1555.

Bursch, W. 2001. The autophagosomal-lysosomal compartment in programmed cell death. *Cell Death Differ.* 8:569–581.

Ciechanover, A., and P. Brundin. 2003. The ubiquitin proteasome system in neurodegenerative diseases: sometimes the chicken, sometimes the egg. *Neuron.* 40:427–446.

Dunn, W.A., Jr. 1994. Autophagy and related mechanisms of lysosome-mediated protein degradation. *Trends Cell Biol.* 4:139–143.

Goldberg, A.L. 2003. Protein degradation and protection against misfolded or damaged proteins. *Nature.* 426:895–899.

Gronostajski, R.M., and A.B. Pardee. 1984. Protein degradation in 3T3 cells and tumorigenic transformed 3T3 cells. *J. Cell. Physiol.* 119:127–132.

Hanaoka, H., T. Noda, Y. Shirano, T. Kato, H. Hayashi, D. Shibata, S. Tabata, and Y. Ohsumi. 2002. Leaf senescence and starvation-induced chlorosis are accelerated by the disruption of an *Arabidopsis* autophagy gene. *Plant Physiol.* 129:1181–1193.

Ichimura, Y., T. Kirisako, T. Takao, Y. Satomi, Y. Shimonishi, N. Ishihara, N. Mizushima, I. Tanida, E. Kominami, M. Ohsumi, et al. 2000. A ubiquitin-like system mediates protein lipidation. *Nature.* 408:488–492.

Kabeya, Y., N. Mizushima, T. Ueno, A. Yamamoto, T. Kirisako, T. Noda, E. Kominami, Y. Ohsumi, and T. Yoshimori. 2000. LC3, a mammalian homologue of yeast Apg8p, is localized in autophagosome membranes after processing. *EMBO J.* 19:5720–5728.

Kabeya, Y., N. Mizushima, A. Yamamoto, S. Oshitani-Okamoto, Y. Ohsumi, and T. Yoshimori. 2004. LC3, GABARAP and GATE16 localize to autophagosomal membrane depending on form-II formation. *J. Cell Sci.* 117:2805–2812.

Klionsky, D.J., and S.D. Emr. 2000. Autophagy as a regulated pathway of cellular degradation. *Science.* 290:1717–1721.

Komatsu, M., I. Tanida, T. Ueno, M. Ohsumi, Y. Ohsumi, and E. Kominami. 2001. The C-terminal region of an Apg7p/Cvt2p is required for homodimerization and is essential for its E1 activity and E1-E2 complex formation. *J. Biol. Chem.* 276:9846–9854.

Kopito, R.R. 2000. Aggresomes, inclusion bodies and protein aggregation. *Trends Cell Biol.* 10:524–530.

Kuhn, R., F. Schwenk, M. Aguet, and K. Rajewsky. 1995. Inducible gene targeting in mice. *Science.* 269:1427–1429.

Kuma, A., M. Hatano, M. Matsui, A. Yamamoto, H. Nakaya, T. Yoshimori, Y. Ohsumi, T. Tokuhisa, and N. Mizushima. 2004. The role of autophagy during the early neonatal starvation period. *Nature.* 432:1032–1036.

Levine, B., and D.J. Klionsky. 2004. Development by self-digestion: molecular mechanisms and biological functions of autophagy. *Dev. Cell.* 6:463–477.

Lewandoski, M., K.M. Wassarman, and G.R. Martin. 1997. Zp3-cre, a transgenic mouse line for the activation or inactivation of loxP-flanked target genes specifically in the female germ line. *Curr. Biol.* 7:148–151.

Liang, X.H., S. Jackson, M. Seaman, K. Brown, B. Kempkes, H. Hibshoosh, and B. Levine. 1999. Induction of autophagy and inhibition of tumorigenesis by beclin 1. *Nature.* 402:672–676.

Massey, A., R. Kiffin, and A.M. Cuervo. 2004. Pathophysiology of chaperone-mediated autophagy. *Int. J. Biochem. Cell Biol.* 36:2420–2434.

Mizushima, N., T. Noda, T. Yoshimori, Y. Tanaka, T. Ishii, M.D. George, D.J. Klionsky, M. Ohsumi, and Y. Ohsumi. 1998. A protein conjugation system essential for autophagy. *Nature.* 395:395–398.

Mizushima, N., A. Yamamoto, M. Hatano, Y. Kobayashi, Y. Kabeya, K. Suzuki, T. Tokuhisa, Y. Ohsumi, and T. Yoshimori. 2001. Dissection of autophagosome formation using Apg5-deficient mouse embryonic stem cells. *J. Cell Biol.* 152:657–668.

Mizushima, N., Y. Ohsumi, and T. Yoshimori. 2002. Autophagosome formation in mammalian cells. *Cell Struct. Funct.* 27:421–429.

Mizushima, N., A. Yamamoto, M. Matsui, T. Yoshimori, and Y. Ohsumi. 2004. In vivo analysis of autophagy in response to nutrient starvation using transgenic mice expressing a fluorescent autophagosome marker. *Mol. Biol. Cell.* 15:1101–1111.

Mortimore, G.E., and A.R. Poso. 1987. Intracellular protein catabolism and its control during nutrient deprivation and supply. *Annu. Rev. Nutr.* 7:539–564.

Murata, S., H. Udono, N. Tanahashi, N. Hamada, K. Watanabe, K. Adachi, T. Yamano, K. Yui, N. Kobayashi, M. Kasahara, et al. 2001. Immunoproteasome assembly and antigen presentation in mice lacking both PA28alpha and PA28beta. *EMBO J.* 20:5898–5907.

Nakagawa, I., A. Amano, N. Mizushima, A. Yamamoto, H. Yamaguchi, T. Kamimoto, A. Nara, J. Funao, M. Nakata, K. Tsuda, et al. 2004. Autophagy defends cells against invading group *A Streptococcus*. *Science.* 306:1037–1040.

Nishino, I., J. Fu, K. Tanji, T. Yamada, S. Shimojo, T. Koori, M. Mora, J.E. Riggs, S.J. Oh, Y. Koga, et al. 2000. Primary LAMP-2 deficiency causes X-linked vacuolar cardiomyopathy and myopathy (Danon disease). *Nature.* 406:906–910.

Notterpek, L., M.C. Ryan, A.R. Tobler, and E.M. Shooter. 1999. PMP22 accumulation in aggresomes: implications for CMT1A pathology. *Neurobiol. Dis.* 6:450–460.

Ohsumi, Y. 2001. Molecular dissection of autophagy: two ubiquitin-like systems. *Nat. Rev. Mol. Cell Biol.* 2:211–216.

Perlmutter, D.H. 2002. Liver injury in alpha1-antitrypsin deficiency: an aggregated protein induces mitochondrial injury. *J. Clin. Invest.* 110:1579–1583.

Qu, X., J. Yu, G. Bhagat, N. Furuya, H. Hibshoosh, A. Troxel, J. Rosen, E.L. Eskelinen, N. Mizushima, Y. Ohsumi, et al. 2003. Promotion of tumorigenesis by heterozygous disruption of the beclin 1 autophagy gene. *J. Clin. Invest.* 112:1809–1820.

Seglen, P.O., and P. Bohley. 1992. Autophagy and other vacuolar protein degradation mechanisms. *Experientia.* 48:158–172.

Shintani, T., and D.J. Klionsky. 2004. Autophagy in health and disease: a double-edged sword. *Science.* 306:990–995.

Shintani, T., N. Mizushima, Y. Ogawa, A. Matsuura, T. Noda, and Y. Ohsumi. 1999. Apg10p, a novel protein-conjugating enzyme essential for autophagy in yeast. *EMBO J.* 18:5234–5241.

Sutovsky, P., R.D. Moreno, J. Ramalho-Santos, T. Dominko, C. Simerly, and G. Schatten. 1999. Ubiquitin tag for sperm mitochondria. *Nature.* 402:371–372.

Tanaka, Y., G. Guhde, A. Suter, E.L. Eskelinen, D. Hartmann, R. Lullmann-Rauch, P.M. Janssen, J. Blanz, K. von Figura, and P. Saftig. 2000. Accumulation of autophagic vacuoles and cardiomyopathy in LAMP-2-deficient mice. *Nature.* 406:902–906.

Tanida, I., N. Mizushima, M. Kiyooka, M. Ohsumi, T. Ueno, Y. Ohsumi, and E. Kominami. 1999. Apg7p/Cvt2p: a novel protein-activating enzyme essential for autophagy. *Mol. Biol. Cell.* 10:1367–1379.

Tanida, I., E. Tanida-Miyake, T. Ueno, and E. Kominami. 2001. The human homolog of *Saccharomyces cerevisiae* Apg7p is a protein-activating enzyme for multiple substrates including human Apg12p, GATE-16, GABARAP, and MAP-LC3. *J. Biol. Chem.* 276:1701–1706.

Tateishi, K., M. Omata, K. Tanaka, and T. Chiba. 2001. The NEDD8 system is essential for cell cycle progression and morphogenetic pathway in mice. *J. Cell Biol.* 155:571–579.

Tsukada, M., and Y. Ohsumi. 1993. Isolation and characterization of autophagy-defective mutants of *Saccharomyces cerevisiae*. *FEBS Lett.* 333:169–174.

Ueno, T., S. Watanabe, M. Hirose, T. Namihisa, and E. Kominami. 1990. Phalloidin-induced accumulation of myosin in rat hepatocytes is caused by suppression of autolysosome formation. *Eur. J. Biochem.* 190:63–69.

Waguri, S., N. Sato, T. Watanabe, K. Ishidoh, E. Kominami, K. Sato, and Y. Uchiyama. 1995. Cysteine proteinases in GH4C1 cells, a rat pituitary tumor cell line, are secreted by the constitutive and regulated secretory pathways. *Eur. J. Cell Biol.* 67:308–318.

Xue, L., G.C. Fletcher, and A.M. Tolkovsky. 1999. Autophagy is activated by apoptotic signalling in sympathetic neurons: an alternative mechanism of death execution. *Mol. Cell. Neurosci.* 14:180–198.

Yue, Z., S. Jin, C. Yang, A.J. Levine, and N. Heintz. 2003. Beclin 1, an autophagy gene essential for early embryonic development, is a haploinsufficient tumor suppressor. *Proc. Natl. Acad. Sci. USA.* 100:15077–15082.

Journal of Neurochemistry, 2005, **94**, 1254–1263 doi:10.1111/j.1471-4159.2005.03272.x

In vivo evidence of CHIP up-regulation attenuating tau aggregation

Naruhiko Sahara,* Miyuki Murayama,* Tatsuya Mizoroki,* Makoto Urushitani,† Yuzuru Imai,† Ryosuke Takahashi,†,[1] Shigeo Murata,‡ Keiji Tanaka‡ and Akihiko Takashima*

**Laboratory for Alzheimer's Disease and †Laboratory for Motor System Neurodegeneration. RIKEN Brain Science Institute, Saitama, Japan*

‡Department of Molecular Oncology, Tokyo Metropolitan Institute of Medical Science, Tokyo, Japan

Abstract

The carboxyl terminus of heat-shock cognate (Hsc)70-interacting protein (CHIP) is a ubiquitin E3 ligase that can collaborate with molecular chaperones to facilitate protein folding and prevent protein aggregation. Previous studies showed that, together with heat-shock protein (Hsp)70, CHIP can regulate tau ubiquitination and degradation in a cell culture system. Ubiquitinated tau is one component in neurofibrillary tangles (NFTs), which are a major histopathological feature of Alzheimer's disease (AD). However, the precise sequence of events leading to NFT formation and the mechanisms involved remain unclear. To confirm CHIP's role in suppressing NFT formation *in vivo*, we performed a quantitative analysis of CHIP in human and mouse brains. We found increased levels of CHIP and Hsp70 in AD compared with normal controls. CHIP levels in both AD and controls corresponded directly to Hsp90 levels, but not to Hsp70 or Hsc70 levels. In AD samples, CHIP was inversely proportional to sarkosyl-insoluble tau accumulation. In a JNPL3 mouse brain tauopathy model, CHIP was widely distributed but weakly expressed in spinal cord, which was the most prominent region for tau inclusions and neuronal loss. Protein levels of CHIP in cerebellar regions of JNPL3 mice were significantly higher than in non-transgenic littermates. Human tau was more highly expressed in this region of mouse brains, but only moderate levels of sarkosyl-insoluble tau were detected. This was confirmed when increased insoluble tau accumulation was found in mice lacking CHIP. These findings suggest that increases in CHIP may protect against NFT formation in the early stages of AD. If confirmed, this would indicate that the quality-control machinery in a neuron might play an important role in retarding the pathogenesis of tauopathies.

Keywords: Alzheimer's disease, carboxyl terminus of heat-shock cognate 70-interacting protein, heat-shock protein, molecular chaperone, neurofibrillary tangle, tau.

J. Neurochem. (2005) **94,** 1254–1263.

The carboxyl terminus of heat-shock cognate (Hsc)70-interacting protein (CHIP) is a key molecule in protein quality-control processes that links the ubiquitin–proteasome and chaperone systems (Murata *et al.* 2001). CHIP has the U-box domain that facilitates ubiquitin-conjugating enzyme (E2)-dependent ubiquitination (Hatakeyama *et al.* 2001). CHIP was originally discovered as a co-chaperone with a tetratricopeptide repeat-containing protein that negatively regulates the ATPase and chaperone activities of Hsc70 (Ballinger *et al.* 1999). The biochemical effects of CHIP have been well characterized using cell culture systems. Various molecules have been identified as CHIP substrates, including the glucocorticoid receptor (Connell *et al.* 2001), the misfolded cystic fibrosis transmembrane-conductance regulator (CFTR) (Meacham *et al.* 2001), heat-denatured luciferase (Murata *et al.* 2001), the transmembrane receptor tyrosine kinase ErbB2 (Xu *et al.* 2002)

Received February 16, 2005; revised manuscript received April 10, 2005; accepted April 26, 2005.

Address correspondence and reprint requests to Akihiko Takashima, Laboratory for Alzheimer's Disease, RIKEN Brain Science Institute, Wako-shi, Saitama 351–0198, Japan. E-mail: kenneth@brain.riken.jp

[1]The present address of Ryosuke Takahashi is the Department of Neurology, Graduate School of Medicine, Kyoto University, 54 Kawahara-cho, Shogoin, Sakyo-ku, Kyoto 606-8507, Japan.

Abbreviations used: AD, Alzheimer's disease; CFTR, cystic fibrosis transmembrane-conductance regulator; CHIP, carboxyl terminus of heat-shock cognate 70-interacting protein; Hsc, heat-shock cognate; HSF1, heat shock factor 1; Hsp, heat-shock protein; MES, 2-(N-Morpholino) ethanesulfonic Acid; NFT, neurofibrillary tangle; NSE, neuron-specific enolase; PAGE, polyacrylamide gel electrophoresis; PBS, phosphate-buffered saline; PHF, paired helical filaments; PHF-tau, PHF-1 antibody-immunoreactive tau; PMSF, phenylmethylsulfonyl fluoride; SDS, sodium dodecyl sulfate; TBS, Tris-buffered saline; Tg, transgenic.

and microtubule-associated protein tau (Petrucelli *et al.* 2004; Shimura *et al.* 2004). We found that CHIP directly mediates tau ubiquitination without heat-shock proteins (Hsps) *in vitro*, preferentially interacts with four-repeat tau, and protects against vulnerability of P301L mutated tau expressing cells (Hatakeyama *et al.* 2004). However, little is known about the biochemical features of CHIP in the brain. Only immunohistochemical analyses have been reported, including those that show anti-CHIP antibody-positive tau inclusions in several tauopathies including Alzheimer's disease (AD), progressive supranuclear palsy, corticobasal degeneration and Pick's disease (Hatakeyama *et al.* 2004; Petrucelli *et al.* 2004), and anti-CHIP antibody-positive Lewy body-like hyaline inclusions in a familial amyotrophic lateral sclerosis mouse model (Urushitani *et al.* 2004).

Tau is a neuronal microtubule-binding protein that normally enhances microtubule stability. However, it can be hyperphosphorylated in pathogenic conditions, and detach from microtubules and accumulate in the neurofibrillary tangles (NFTs) that are one of neuropathological hallmarks of AD (Grundke-Iqbal *et al.* 1986). Despite the suspected role of tau phosphorylation in NFT formation, the precise sequence of events leading to NFT formation and the mechanisms involved remain poorly understood. In addition to tau phosphorylation, other abnormal post-translational modifications have been observed including ubiquitination, glycosylation, glycation, polyamination, nitration and proteolysis (for review, see Gong *et al.* 2005). In most neurodegenerative diseases, anti-ubiquitin antibody- and anti-proteasome antibody-positive inclusions were detected in affected neurons (for review, see Sherman and Goldberg 2001), so the ubiquitin–proteasome may be one mechanism responsible for tau degradation in tauopathies. Various molecular chaperones were also colocalized in protein aggregates that are characteristic of neurodegenerative diseases (for review, see Muchowski and Wacker 2005). CHIP may attenuate NFT formation as a bridging mechanism between molecular chaperones and the ubiquitin–proteasome system.

In the present study, human AD brain, JNPL3 mice (Lewis *et al.* 2000) expressing human P301L mutant tau that is associated with frontotemporal dementia and parkinsonism linked to chromosome 17, and a novel *CHIP* knockout mouse were used to investigate the *in vivo* roles of CHIP in regulating tau ubiquitination, degradation and aggregation. We found increased levels of CHIP in AD brains that were inversely proportional to the amount of accumulated tau. The level of CHIP corresponded with the level of Hsp90 but not with that of Hsp70 or Hsc70. These *in vivo* studies of CHIP biochemistry suggest the existence of a Hsp90–CHIP chaperone system, which plays an ameliorating role in the early stages of tauopathies.

Materials and methods

Antibodies

Polyclonal CHIP antibodies (R1) were prepared in rabbits (Imai *et al.* 2002). Antiserum specific for recombinant CHIP with a His-Tag sequence was purchased from Calbiochem (La Jolla, CA, USA). E1 (Kenessey *et al.* 1997), a polyclonal antibody specific to human tau (amino acids 19–33, according to the numbering of a longest isoform of human tau unphosphorylated), was prepared in our laboratory. Polyclonal tau antibody tauC was raised against tau polypeptide corresponding to amino acid residues 422–438. Anti-Tau5 and pS199 (phosphorylation site at Ser199) were purchased from Biosource International (Camarillo, CA, USA). Anti-Tau1 was from Chemicon (Temecula, CA, USA). Monoclonal antibody to tau phosphorylated at ser396/Ser404 (PHF-1) was provided by Dr Peter Davies (Jicha *et al.* 1999). Monoclonal antibodies to Hsp90, Hsp70, β-actin, neuron-specific enolase (NSE) and ubiquitin were purchased from Santa Cruz Biotechnology (Santa Cruz, CA, USA), Chemicon, Sigma (St Louis, MO, USA) Upstate (Charlottesville, VA, USA) and MBL (Nagoya, Japan) respectively. Polyclonal antibody to Hsc70 was purchased from MBL. For western blotting, antibodies were used at the following dilutions in blocking solution: CHIP, 1 : 5000; E1, 1 : 5000; tauC, 1 : 5000; tau1, 1 : 2000; tau5, 1 : 2000; pS199, 1 : 5000; PHF-1, 1 : 2000; Hsp90, 1 : 2000; Hsp70, 1 : 1000; β-actin, 1 : 10 000; NSE, 1 : 1000; ubiquitin, 1 : 500; Hsc70, 1 : 1000.

Human brain

Temporal cortices from nine AD (AD1 to AD9) and six non-AD controls (C1 to C6) were obtained. They were processed for western blotting as described below. The age, sex and post-mortem intervals of each subject were: AD2, 85 years, male, 10 h; AD3, 77 years, female, 2.5 h; AD4, 66 years, female, 2.5 h; AD5, 79 years, male, 1.5 h; AD7, 66 years, male, 2.5 h; AD8, 60 years, female, 3 h; C1, 57 years, female, 8 h; C2, 69 years, male; C3, 69 years, male; C4, 68 years, male, 6 h; C6, 65 years, female. Information about remaining samples was not available (described in Yan *et al.* 1994).

JNPL3 mice and littermates

Female hemizygous JNPL3 mice (Tau MI with B6D2F1 background; Taconic Laboratories Germantown, NY, USA) were obtained at 8 weeks of age. JNPL3 mice express the 4R0N isoform of human P301L mutant tau and are characterized as developing NFTs, as well as sarkosyl-insoluble tau in an age-dependent manner (Lewis *et al.* 2001; Sahara *et al.* 2002). Transgenic (Tg) mice and non-Tg littermates were bred by mating hemizygous JNPL3 mice with C57BL/6J Jcl (Clea, Tokyo, Japan). Mice were genotyped for the *tau* transgene by PCR between exons 9 and 13 of human tau cDNA. Animals were housed under controlled conditions with a 12-h day–night cycle. They were killed between 1.5 and 11.6 months after birth. The age ranges of the JNPL3 mice were 1.5 months ($n = 2$), 4–5 months ($n = 2$), 6–7 months ($n = 3$), 8–9 months ($n = 3$) and 10–11 months ($n = 2$). The age ranges of non-Tg mice were 1.5 months ($n = 1$), 4–5 months ($n = 3$), 6–7 months ($n = 2$) and 8–9 months ($n = 3$). Procedures involving animals and their care were approved by the Animal Care and Use Committee of RIKEN.

Tissue extraction

Mouse brains were separated into eight regions: olfactory bulb, cerebral cortex, hippocampus, diencephalons, midbrain, pons and medulla oblongata, cerebellum and spinal cord. These regions were quickly frozen on dry ice and stored at −80°C. Each sample was homogenized subsequently in five volumes of Tris-buffered saline (TBS) containing protease and phosphatase inhibitors [25 mM Tris/HCl, pH 7.4, 150 mM NaCl, 1 mM EDTA, 1 mM EGTA, 5 mM sodium pyrophosphate, 30 mM β-glycerophosphate, 30 mM sodium fluoride and 1 mM phenylmethylsulfonyl fluoride (PMSF)]. The homogenates were centrifuged at 27 000 *g* for 15 min at 4°C to obtain a supernatant (TBS sup) and pellet fractions. Pellets were re-homogenized in five volumes of high-salt/sucrose buffer (0.8 M NaCl, 10% sucrose, 10 mM Tris/HCl, pH 7.4, 1 mM EGTA, 1 mM PMSF) and centrifuged as above. The supernatants were collected and incubated with sarkosyl (Sigma; 1% final concentration) for 1 h at 37°C, followed by centrifugation at 150 000 *g* for 1 h at 4°C to obtain salt and sarkosyl-soluble and sarkosyl-insoluble pellets (srk-ppt fractions). To determine the extent of post-mortem protein degradation, hemibrains were kept at room temperature (25°C) for various time intervals (1, 2, 4, 8, 24 and 70 h) after the death of 7-month-old female C57BL/6J mice. As a control, the other hemibrains were quickly frozen in dry ice and stored at −80°C. Each sample was homogenized in TBS buffer containing protease and phosphatase inhibitors, and was centrifuged at 27 000 *g* for 15 min at 4°C. The supernatants were used for western blot analysis.

CHIP knockout mice

The first six exons of the *CHIP* gene were replaced with a PGK-neo selection cassette by homologous recombination. Germline transfer of the targeted allele was successful. Mice heterozygous at the *CHIP* locus were maintained on a C57BL/6 background. Mice aged 2.5 months (wild type $n = 1$, heterozygous $n = 1$, homozygous $n = 1$) and 18 months (wild type $n = 4$, heterozygous $n = 4$, homozygous $n = 4$) were killed, and hemibrains were quickly frozen on dry ice and stored at −80°C. As described previously (Ishihara *et al.* 1999; Tanemura *et al.* 2002), tissue extracts were sequentially fractionated with the following buffers: reassembly buffer (RAB; 0.1 M 2-(N-Morpholino)ethanesulfonic Acid (MES), 1 mM EGTA, 0.5 mM $MgSO_4$, 0.75 M NaCl, 0.02 M NaF, 1 mM PMSF and protease inhibitor cocktail, pH 7.0), RAB containing 1 M sucrose, RIPA buffer [50 mM Tris, 150 mM NaCl, 1% NP-40, 5 mM EDTA, 0.5% sodium deoxycholate and 0.1% sodium dodecyl sulfate (SDS), pH 8.0], RIPA buffer containing 1% SDS, and TBS containing 1% SDS. The final pellet was solubilized in 70% formic acid and reconstituted in Laemmli SDS–polyacrylamide gel electrophoresis (PAGE) sample buffer after lyophilization.

Western blotting

Fractionated tissue extracts were dissolved in sample buffer containing β-mercaptoethanol (0.01%). The boiled extracts were separated by gel electrophoresis on 10% or 4–20% gradient SDS–PAGE gels, and transferred to nitrocellulose membranes (Schleicher & Schuell BioScience, Dassel, Germany). After blocking with a blocking solution containing 5% non-fat milk, 0.1% goat serum and 0.1% Tween-20 in phosphate-buffered saline (PBS), the membranes were incubated with various antibodies, washed to remove excess antibodies, and then incubated with peroxidase-conjugated goat anti-rabbit antibodies (1 : 5000; Jackson ImmunoResearch, West Grove, PA, USA) or anti-mouse IgG (1 : 5000; Jackson ImmunoResearch). Bound antibodies were detected using an enhanced chemiluminescence system, SuperSignal West Pico (Pierce Biotechnology, Rockford, IL, USA). For specificity testing of anti-CHIP antibody, pre-absorption was performed. Recombinant His-tagged CHIP was resuspended in 1% bovine serum albumin, 0.1% goat serum and 0.1% Tween-20 in PBS to a concentration of 40 μg/mL. The solution was added to dilute CHIP antibody to a final dilution of 1 : 5000. The mixture was rotated for 2 h at room temperature, then centrifuged at 12 000 *g* for 5 min. The supernatant was separated from the pellet and used for western blotting. Quantitation and visual analysis of immunoreactivity were performed with a computer-linked LAS-1000 Bio-Imaging Analyzer System (Fujifilm, Tokyo, Japan) using the software program Image Gauge 3.0 (Fujifilm).

Statistical analysis

The correlation between the levels of CHIP in AD brain and control brain, and between CHIP and Hsp levels, was tested by unpaired *t*-test with Welch correction. The correlation between the level of CHIP and PHF-tau was tested using Pearson correlation. Data were analyzed with InStat for Macintosh, version 3.0a (Graphpad, San Diego, CA, USA). The level of significance was set at $p < 0.05$.

Results

Identification of CHIP in brain extracts

CHIP, a 35-kDa cytoplasmic protein, is highly expressed in adult striated muscle with less expression in the pancreas and brain. It is also expressed broadly in tissue culture (Ballinger *et al.* 1999). Polyclonal CHIP antibodies from both laboratory and commercial sources were used for western blotting. Both were raised from full-length CHIP recombinant protein. Samples from human embryonic kidney (HEK)293 cells showed the strongest immunoreactive band with a mobility size of 35 kDa (Fig. 1a). Both mouse and human brain extracts showed a single 35-kDa band in the blot with R1 antibody. This band was absorbed by preincubation of primary antibody with recombinant protein. The blot with the Calbiochem antibody showed a 35-kDa band of the same intensity in each sample, but additional bands were detected. These data suggest that the 35-kDa band was the protein product of *CHIP* and that the R1 antibody is more specific to CHIP than the antibody from Calbiochem. We also detected doublet bands in human materials using the enlarged electrophoretic condition (Fig. 1b). For quantitative analysis, we excluded the upper band in human materials because the mobility of the lower band was same as the 35-kDa band in mouse brain (Fig. 1b) and all the human brain samples showed similar extensions of the upper band (Fig. 2a).

Levels of CHIP in AD brain were higher than levels in non-AD controls

Quantitative western blotting analyses revealed variable levels of the 35-kDa band in human brain extracts (Fig. 2a).

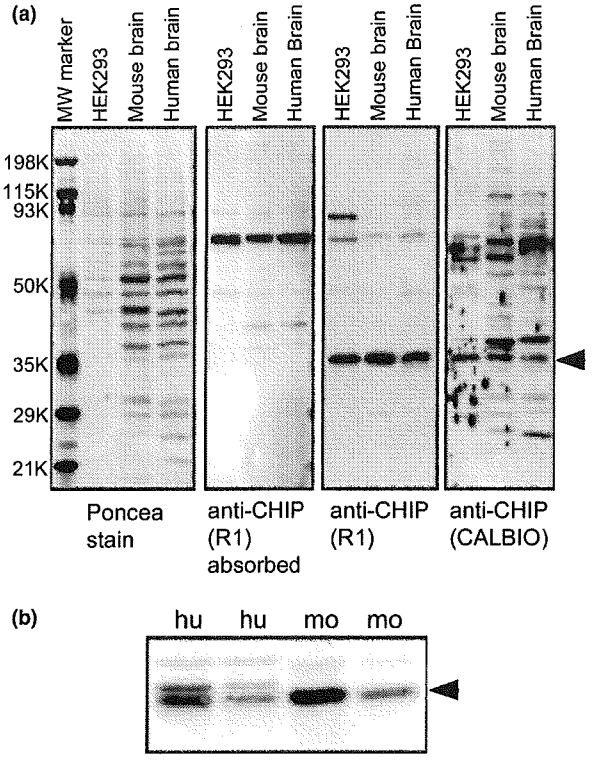

Fig. 1 Identification of CHIP using specific antibodies. (a) Replicated membranes containing human embryonic kidney (HEK)293 cells, mouse brain and human brain extracts were immunoblotted with anti-CHIP antibodies [preabsorbed R1, R1 and Calbiochem (CALBIO)]. One set of membranes was stained with poncea. A 35-kDa band (arrowhead) was detected with both R1 and Calbiochem antibodies but completely absorbed by recombinant CHIP. (b) Human brain extracts contained doublet bands. The lower band in human brain indicated by arrowhead was identical to the band in mouse brain.

Before making comparisons between AD and non-AD controls, both sarkosyl-insoluble tau and SDS-insoluble β-amyloid were analyzed by western blotting to confirm diagnostic information. PHF-1-positive triplet bands were detected in all nine AD cases but not in the non-AD controls when sarkosyl-insoluble fractions derived from over 40 mg wet-weight of brain tissue were loaded (data not shown). SDS-insoluble β-amyloid was detected in all AD cases and some non-AD controls (data not shown). To compare protein levels of CHIP and Hsp between AD and non-AD controls, the amount of β-actin was used for normalization of protein levels. Levels of CHIP were significantly higher in AD brain compared with non-AD controls ($p = 0.040$; unpaired t-test with Welch correction) (Fig. 2b). A significant increase in Hsp70 levels in AD compared with control brains was observed ($p = 0.0032$) (Fig. 2d), but no significant difference in either Hsp90 or Hsc70 ($p = 0.84$ and $p = 0.57$ respectively) (Fig. 2c). Comparing individual samples, CHIP and Hsp90 levels were directly related, but CHP levels were not related to those of either Hsp70 or Hsc70 (Figs 2a and e). The correlation between the levels of CHIP and Hsp90 was highly significant ($r = 0.71$, $p = 0.0029$, $n = 15$; Pearson correlation). When the amount of NSE was used for normalization, the same statistical results were obtained (data not shown).

Inverse relationship between CHIP and PHF-1 antibody-immunoreactive tau (PHF-tau) in AD brain

To determine whether NFT formation in AD brain is influenced by the protein level of CHIP, the amount of CHIP, normalized with respect to β-actin in the TBS-soluble fraction, was plotted against PHF-tau in the sarkosyl-insoluble fraction. These were samples that tested positive for highly phosphorylated tau. Although detailed information on the pathological course for each AD case was not available, the relative amount of PHF-tau revealed through biochemical studies provided detailed information about the NFT pathogenesis in each. This information correlated with the severity of disease (Dickson *et al.* 2000; Johnson and Bailey 2002). As shown in Fig. 2(a), the intensity of PHF-tau staining varied among the AD cases as did that of both CHIP and Hsp90. Interestingly, the amount of PHF-tau was inversely proportional to amount of CHIP ($r = -0.83$, $p = 0.0051$, $n = 9$; Pearson correlation) (Fig. 2f). As described previously, levels of Hsp90 in AD cases with mature PHF-tau accumulation were lower than those in immature or non-AD cases (Dou *et al.* 2003). Conversely, soluble tau levels were not influenced by either CHIP or Hsp90 levels. To determine whether the sequestration of CHIP with NFTs occurred during pathogenesis, we analyzed CHIP levels in the sarkosyl-insoluble fraction (Fig. 2a). Consistent with the results of the anti-CHIP blot of the TBS sup fraction, the level of sarkosyl-insoluble CHIP was inversely related to the PHF-tau level. Sarkosyl-insoluble CHIP in controls was also detected with similar intensity to that in AD cases. These data suggest that CHIP precipitated in this fraction in a PHF-tau-independent manner.

Effect of post-mortem interval on protein levels of CHIP

Large variations in CHIP and Hsp90 protein levels were found among control and AD brains (Fig. 2a). To exclude the possibility of post-mortem protein degradation, we attempted the comparative protein quantification of mouse brains with several post-mortem intervals. Coomassie Brilliant Blue staining of polyacrylamide gels showed visible protein degradation after a post-mortem interval of 24 h (Fig. 3). However, western blots for CHIP, Hsp90, Hsp70 and β-actin showed constant protein levels. Only tau protein levels were affected by the post-mortem interval. The observed mobility shift may correspond to dephosphorylation. These data strongly suggest that protein levels of CHIP and Hsps extracted from both human and mouse brains were not affected by the post-mortem interval.

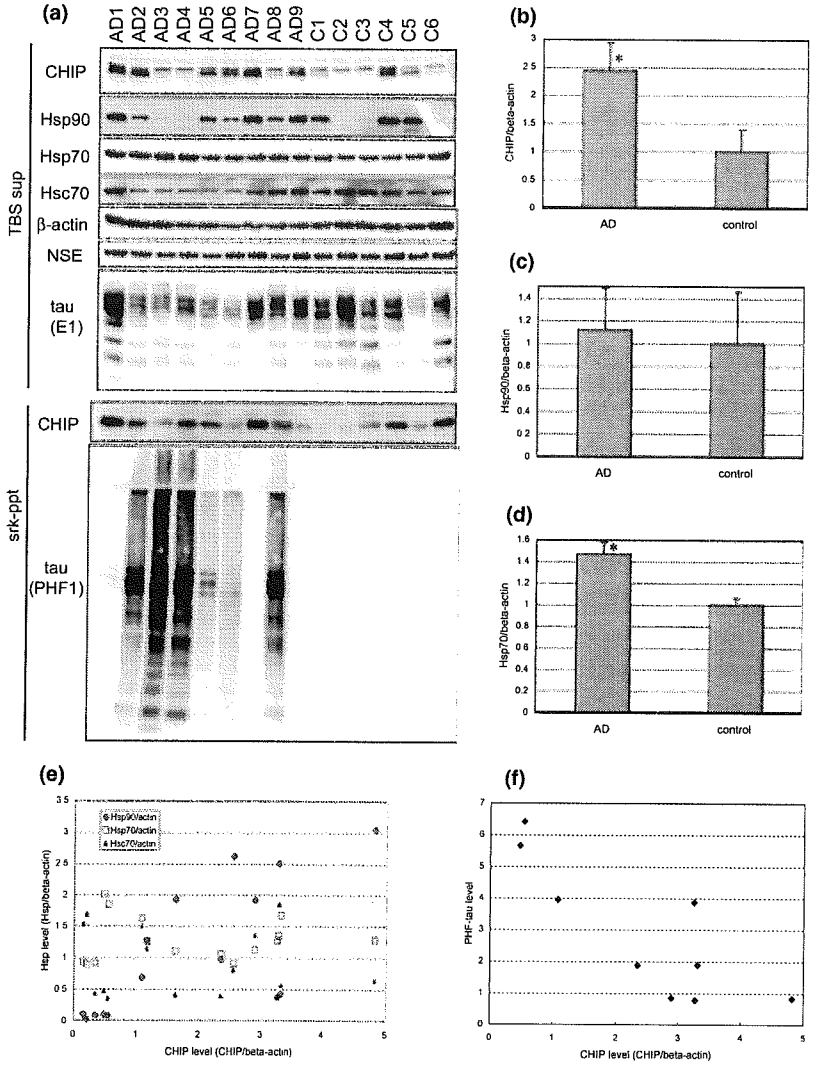

Fig. 2 Quantitative analysis of CHIP in human brains. (a) TBS-soluble fractions (TBS sup) from human temporal cortex from nine AD and six non-AD control cases were blotted using CHIP (R1), Hsp90, Hsp70, Hsc70, β-actin, NSE and E1 antibodies. Sarkosyl-insoluble fractions (srk-ppt) derived from 40 mg wet-weight of brain were blotted using CHIP (R1) antibodies and those derived from 4 mg wet-weight of brain were blotted using PHF-1 antibody. Amounts of CHIP (b), Hsp90 (c) and Hsp70 (d) normalized with respect to β-actin were analyzed. Values are mean ± SEM. $^*p < 0.05$ versus control (unpaired *t*-test with Welch correction). (e) Correlations between CHIP and Hsp90, Hsp70 or Hsc70 levels. (f) Amount of CHIP normalized with respect to β-actin in TBS-soluble fraction plotted against sarkosyl-insoluble PHF-tau level. $p < 0.01$ ($n = 9$; Pearson correlation).

Distribution of CHIP in mouse brain

Since the discovery of CHIP (Ballinger *et al.* 1999) and its role as E3 ligase (Hatakeyama *et al.* 2001; Jiang *et al.* 2001; Murata *et al.* 2001), little research has been conducted to determine its *in vivo* protein properties. In the present study the distribution of CHIP in mouse brain was investigated using biochemical strategies. CHIP was found to be highly expressed in the olfactory bulb, cerebral cortex, hippocampus and cerebellum, moderately expressed in the diencephalons, midbrain and pons/medulla oblongata, but weakly expressed in the spinal cord (Fig. 4a). Hsp90 was broadly expressed throughout the mouse brain, whereas Hsp70 was highly expressed in cerebral cortex and hippocampus with only moderate expression in other brain regions (Fig. 4a). The distribution patterns of the three chaperone-related proteins in mouse samples were not identical. CHIP distribution in mouse brain corresponded with tau distribution except in the olfactory bulb. The distribution patterns of CHIP, Hsp90 and Hsp70 did not vary with age or sex (data not shown).

Increased level of CHIP in JNPL3 mouse brain

To search for linkages between abnormal tau accumulation and CHIP expression, JNPL3 mouse brains were analyzed; 64-kDa tau was observed in the sarkosyl-insoluble fraction from the midbrain, pons/medulla oblongata and spinal cord regions of 9.5-month-old female JNPL3 mouse (Fig. 4b, middle panel). As described previously (Sahara *et al.* 2002), human P301L tau protein expression was higher in the hindbrain regions, including midbrain, pons/medulla oblongata, cerebellum and spinal cord, than in the forebrain regions, including cerebral cortex, hippocampus and diencephalons (Fig. 4b, upper panel). Interestingly, the cerebellum had the highest levels of exogenous tau protein but only moderate levels of sarkosyl-insoluble tau. The distribution pattern of

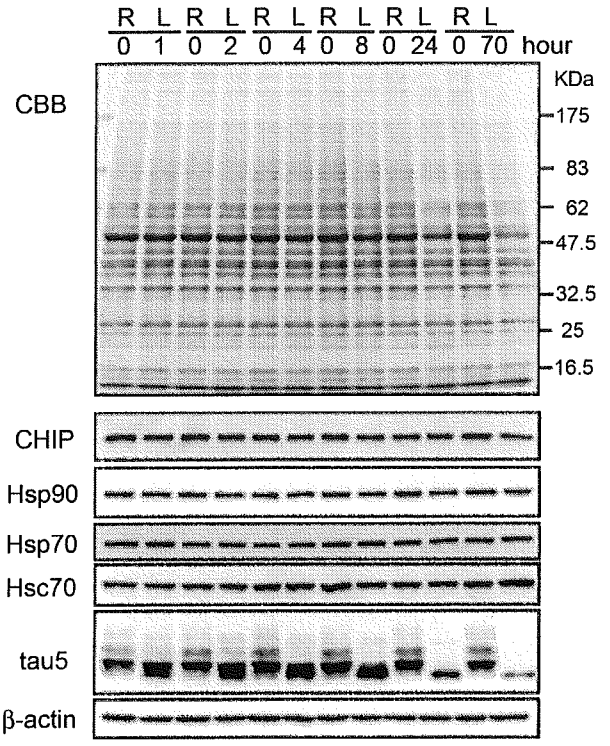

Fig. 3 Effect of post-mortem interval on protein degradation in mouse brains. TBS-soluble fractions from mouse hemibrains were separated by SDS–PAGE then immunoblotted using CHIP, Hsp90, Hsp70, Hsc70, tau5 and β-actin antibodies. One hemibrain (R) was quickly frozen and stored at − 80°C (post-mortem interval zero). The other (L) was kept at room temperature for 1, 2, 4, 8, 24 or 70 h after death. Equal volumes of samples derived from 0.33 mg wet-weight tissue were resolved by SDS–PAGE. Upper panel shows Coomassie Brilliant Blue (CBB) staining with molecular weight markers.

CHIP in JNPL3 mouse brain was similar to that in wild type (compare Fig. 4b with Fig. 4a). The level of CHIP in spinal cord was only 20% of that in cerebellum. The level of sarkosyl-insoluble tau was inversely related to CHIP levels in cerebellum and spinal cord. Because amounts of sarkosyl-insoluble tau were inversely related to the amount of CHIP in AD brains, we checked the CHIP levels in both cerebellum and spinal cord regions. CHIP levels were more than 15% higher in JNPL3 mouse cerebellar regions than those in non-Tg mouse cerebellar regions, but no difference was found in the levels in the spinal cords of JNPL3 and non-Tg mice when protein levels were normalized with respect to β-actin (cerebellum, $p = 0.023$; spinal cord, $p = 0.49$) (Fig. 4c). Neuronal loss in the spinal cord of JNPL3 mice (Lewis *et al.* 2000) was confirmed by checking the protein levels of NSE as a marker. As shown in Fig. 4(e), the NSE level was significantly lower in JNPL3 mouse spinal cord ($p = 0.0035$). When CHIP levels were normalized with respect to NSE, the levels in JNPL3 mouse spinal cords were higher than those in non-Tg mouse spinal cords but the difference was not significant different ($p = 0.10$) (Fig. 4d).

As the development of tau pathology in the JNPL3 mouse is age dependent, we checked the levels of both CHIP and Hsp90 at different ages. By 11 months of age, the CHIP level in spinal cord was slightly increased but the Hsp90 level was not (Fig. 5a). In cerebellum, no significant differences in either CHIP or Hsp90 levels were found during ageing (Fig. 5b). Although 64-kDa tau was detected in JNPL3 mouse cerebellum, the accumulation of sarkosyl-insoluble tau in spinal cord was greater than that in cerebellum. These data suggest that overexpression of P301L tau increases the amount of CHIP which then attenuates NFT formation, although sufficient levels of CHIP are not produced in spinal cord.

Increased level of insoluble tau in aged *CHIP–/–* mouse brain

Unlike the CHIP-deficient mice described by Dai *et al.* (2003), our *CHIP–/–* mice showed significant anatomical abnormalities such as lower bodyweight and dysbasia. Some 95% of *CHIP–/–* mice die by the third week after birth. The remaining mice survive for more than 1 year. These phenotypes might be due to their genetic backgrounds because our heterozygous mice were maintained on a C57BL/6 strain and back-crossed over five times (Murata S. *et al.*, unpublished observation). We first analyzed the involvement of CHIP in tau phosphorylation and degradation using 2.5- and 18-month-old mouse brains. There were no significant differences in the amounts of soluble tau or tau phosphorylation between wild-type and CHIP-deficient mice (Fig. 6a). We analyzed the solubility of tau protein by extracting brains using buffers with increasing extraction strengths to determine whether tau becomes insoluble in CHIP-deficient mice. Interestingly, both aged *CHIP–/–* and heterozygous (*CHIP+/–*) mouse brains showed increased levels of SDS-insoluble tau, detected by both phosphorylation-independent and -dependent tau antibodies (Fig. 6a). Three additional 18-month-old *CHIP–/–*, *CHIP+/–* and *CHIP+/+* mouse brains were analyzed for insoluble tau accumulation. Although the amount of SDS-insoluble tau varied, it tended to increase with greater CHIP deficiency (Fig. 6c). When we quantified the protein levels of CHIP, heterozygous mouse brains had only 6% of that found in wild-type mouse brains (Fig. 6b). These data suggest that suppression of CHIP induces abnormal tau accumulation in a phosphorylation-independent manner in aged mice.

Discussion

Previous studies have linked CHIP with tau ubiquitination and degradation (Hatakeyama *et al.* 2004; Petrucelli *et al.* 2004; Shimura *et al.* 2004). In this report, we describe the biochemical features of CHIP in human and mouse brain. An

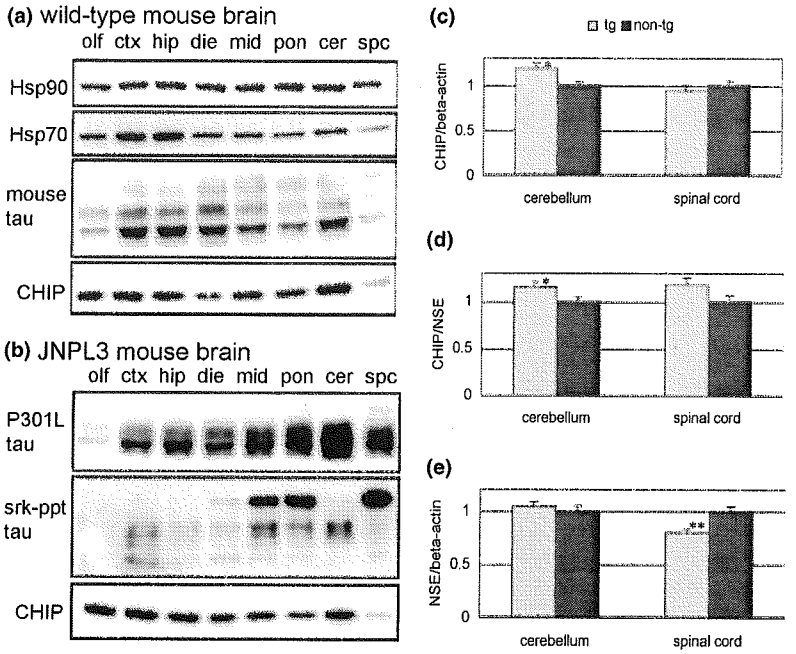

Fig. 4 CHIP distribution in wild-type and JNPL3 mouse brain. (a) TBS-soluble fractions prepared from olfactory bulb (olf), cerebral cortex (ctx), hippocampus (hip), diencephalons (die), midbrain (mid), pons and medulla oblongata (pon), cerebellum (cer) and spinal cord (spc) of 9.3-month-old female mouse were immunoblotted using Hsp90, Hsp70, tau5 and CHIP (R1) antibodies. Equal volumes of samples based on wet weight was resolved by SDS–PAGE. (b) TBS-soluble fractions prepared from the same regions of 9.3-month-old female JNPL3 mouse were blotted using E1 and CHIP (R1) antibodies (top and bottom panel respectively). Sarkosyl-insoluble fractions (srk-ppt) derived from 5 mg wet-weight of each brain region was blotted using E1 antibody (middle). Amounts of CHIP normalized with respect to β-actin (c) and NSE (d), and NSE normalized with respect to β-actin, in cerebellum and spinal cord from Tg (4–10-month-old females, $n = 8$) and non-Tg littermates (females, $n = 8$). Values are mean ± SEM. $^{*}p < 0.05$, $^{**}p < 0.01$ versus non-Tg (unpaired *t*-test with Welch correlation).

increased level of CHIP in AD brain, with respect to controls, was observed. When we analyzed individual differences, the protein levels of CHIP corresponded with Hsp90 levels. An inverse relationship between tau aggregation and CHIP levels was observed in humans and in our mice with tauopathy. We found that a lack of CHIP influenced insoluble tau accumulation. These data suggest that CHIP may protect against tau aggregation and NFT formation.

CHIP is a ubiquitin protein ligase that selectively ubiquitinates denatured proteins when the substrate is captured by a molecular chaperone, including Hsp90 or Hsc70 (Murata *et al.* 2001). Involvement of Hsc70 in the CHIP-dependent ubiquitination of CFTR was also reported (Meacham *et al.* 2001). Connell *et al.* (2001) noted that the ubiquitination-dependent instability of the Hsp90-trapped glucocorticoid receptor was promoted by CHIP. Dai *et al.* (2003) reported that CHIP regulates the activation of Hsp70 by inducing trimerization and transcriptional activation of heat shock factor 1 (HSF-1). Petrucelli *et al.* (2004) found that Hsp70 could reduce tau levels in both a cell culture system and mouse brain. We present novel evidence that levels of Hsp90 correspond to CHIP levels in aged human brains. As Hsp90 often pairs with Hsc/Hsp70, the two chaperones are often thought to be part of a single multichaperone machine (for review, see Young *et al.* 2001), but accumulating evidence suggests that both also work alone. In addition to our CHIP/Hsp90 response, up-regulation of Hsp70 in AD brains has also been reported (Yoo *et al.* 1999). This suggests that in the human brain CHIP might modulate this machinery by interacting directly, and specifically, with either protein in response to the nature of protein misfolding and aggregation.

Immunohistochemical studies found CHIP co-localized with tau-positive lesions in neurons and glia (Petrucelli *et al.* 2004). The number of CHIP-immunoreactive lesions was 50–70% for Pick's disease, 5–10% for AD and 1–5% for both progressive supranuclear palsy and corticobasal degeneration in these studies when CHIP was confirmed using a CHIP-specific antibody with peptide pre-absorption. In contrast, we reported that anti-CHIP antibody stained NFT-bearing cells in progressive supranuclear palsy brain, but only faintly in AD (Hatakeyama *et al.* 2004). This discrepancy might be due to the different specificities of the antibodies. We produced CHIP antibodies from recombinant proteins and confirmed their specificity by western blotting (Fig. 1). Our biochemical observation showed that the amounts of sarkosyl-insoluble tau did not correspond to

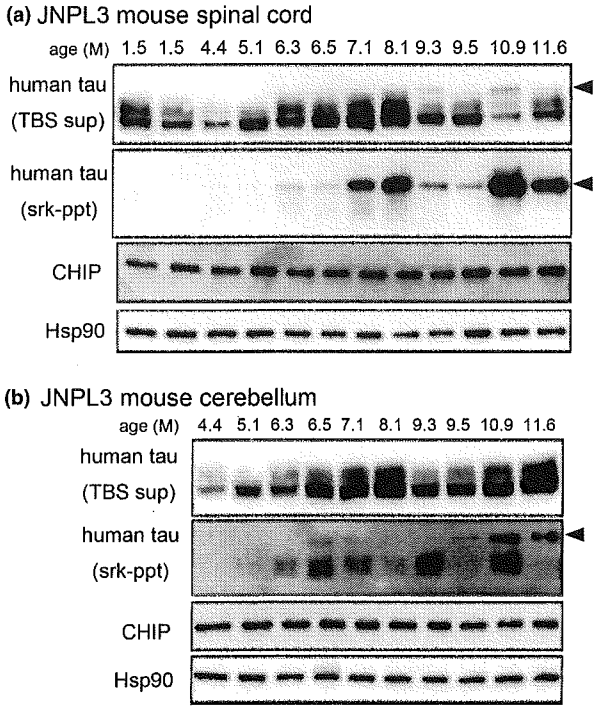

Fig. 5 Changes in CHIP and Hsp90 levels in JNPL3 mouse spinal cord and cerebellum with age. (a) Samples from spinal cords of 1.5–11.6-month (M)-old female JNPL3 mice were analyzed. TBS-soluble fractions (TBS sup) were immunoblotted using E1, CHIP and Hsp90 antibodies. The second panel from the top shows sarkosyl-insoluble fractions (srk-ppt) blotted with E1 antibody (note that the exposure time was shorter than that used for middle panel of Fig. 4b). Equal volumes, based on wet weight, of each sample were resolved by SDS–PAGE. The 64-kDa band (arrowhead) was detected by the E1 antibody in both TBS sup and srk-ppt. (b) Samples from cerebellum of 4.4–11.6-month-old female JNPL3 mice. TBS-soluble fractions (TBS sup) were immunoblotted using E1, CHIP and Hsp90 antibodies. The second panel from the top shows sarkosyl-insoluble fractions (srk-ppt) blotted with E1 antibody (note that the exposure time was much longer than for second panel from top in Fig. 5a).

CHIP levels in NFT-enriched fractions (Fig. 2a). If a direct association between CHIP and Hsp90 can be confirmed, the previous report showing an inverse relationship between aggregated tau and the level of Hsp90 in tau Tg mice and AD brains (Dou *et al.* 2003) will support our observations. The reduction in the levels of CHIP/Hsp90 may stem from the degradation of these proteins together with maturing tau aggregation by a lysosomal pathway or other mechanism. Although more precise experiments are required to confirm the sequestration of CHIP with tau inclusions, we suspect that CHIP expression is up-regulated to cooperate with molecular chaperones for suppression of NFT formation at the early stage of AD.

Here, we quantified CHIP levels in JNPL3 mouse brains in which P301L tau is overexpressed. We observed increased levels of CHIP in the cerebellar regions of JNPL3 mice when compared with age-matched non-Tg littermates and that cerebellar regions of JNPL3 mice had less sarkosyl-insoluble tau than spinal cords, whereas the total tau levels in cerebellum were higher than those in spinal cords (Fig. 4). The finding that the cerebellum had less sarkosyl-insoluble tau than the spinal cord does not contradict the original observations of the pathological features in JNPL3 mouse brain (Lewis *et al.* 2001). We observed that age-dependent hyperphosphorylated tau accumulation in cerebellum of JNPL3 mice was delayed (Fig. 5). In AD, NFTs are observed in the hippocampus and neocortex but not the cerebellum (Larner 1997). Previously, we reported that hyperphosphorylation of tau after changes in glucose metabolism was lower in the cerebellum than in the hippocampus and cerebral cortex (Planel *et al.* 2004). Both CHIP expression and resistance of tau hyperphosphorylation may attenuate abnormal tau accumulation in mouse cerebellum. Because an inverse accumulation of sarkosyl-insoluble tau with CHIP levels, but not Hsp levels, was observed in the mouse brain, CHIP might be essential in preventing prevent tau aggregation whereas Hsp90 and Hsp70 have additional functions in many cellular processes, including protein folding, transport, degradation and signal transduction. The inconsistency between humans and mice might be explained by brain regional differences. To determine whether Hsp90 cooperates with CHIP to prevent tau aggregation in mouse brain, a model that develops tau pathology in cerebral cortex such as the human P301S tau Tg mouse would be more useful (Allen *et al.* 2002). In contrast to human AD brains, which showed massive accumulation of PHF-tau and reduced levels of CHIP, we found no reduction in CHIP levels in either cerebellum or spinal cord of aged JNPL3 mice. It is possible that unknown ubiquitin ligases other than CHIP might be reduced in these brain regions. Further studies are necessary to determine what other factors might be responsible for tau aggregation in JNPL3 mice.

The biochemical analysis of tau in the *CHIP* knockout mouse brains revealed a slight increase in detergent-insoluble tau with no change in the total amount of tau. This indicates that, although eliminating CHIP is not sufficient to induce NFT formation, a lack of CHIP is involved is NFT formation when tau abnormalities are present. As the precise roles of the chaperone system and the ubiquitin proteasomal system within the pathogenesis of tauopathies have yet to be determined, cross-breeding the *CHIP* knockout mouse with a tau Tg mouse may be beneficial.

To our knowledge, this is the first *in vivo* study of CHIP's properties. We confirmed that co-chaperone CHIP was up-regulated by early NFT formation and prevented tau aggregation with the help of molecular chaperones in human and mouse brains. Therefore, CHIP can modify the disease states of human tauopathies when working in combination with its molecular chaperones.

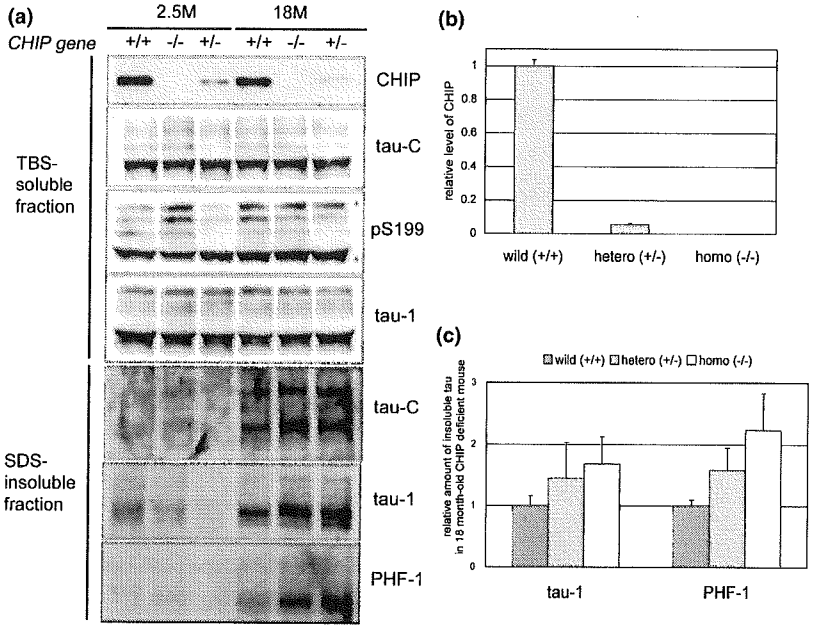

Fig. 6 Insoluble tau accumulation in *CHIP* knockout mouse brain. (a) TBS-soluble fractions derived from 2.5- and 18-month (M)-old *CHIP+/+*, *CHIP+/–* and *CHIP–/–* mouse brains were immunoblotted using CHIP (R1), tauC, pS199 and tau-1 antibodies. SDS-insoluble fractions extracted with 70% formic acid were immunoblotted using tauC, tau1 and PHF-1 antibodies. Samples containing equal amounts of protein were resolved by SDS–PAGE. (b) Relative levels of CHIP in 18-month-old mouse brains ($n = 3$). Values are mean ± SEM with respect to levels in wild-type mice. (c) Amounts of insoluble tau in 18-month-old mouse brains ($n = 3$). SDS-insoluble fractions extracted with 70% formic acid were immunoblotted using tau1 and PHF-1 antibodies, then quantified by means of an image analyzer. Values are mean ± SEM with respect to levels in wild-type mice.

Acknowledgements

This work was supported by research grants from RIKEN Brain Science Institute and a Grant-in-Aid for Scientific Research (Japan Ministry of Education, Culture, Sports, Science and Technology). We are grateful to Bonnie Lee La Madeleine for editing this manuscript.

References

Allen B., Ingram E., Takao M. *et al.* (2002) Abundant tau filaments and nonapoptotic neurodegeneration in transgenic mice expressing human P301S tau protein. *J. Neurosci.* **22**, 9340–9351.

Ballinger C. A., Connell P., Wu Y., Hu Z., Thompson L. J., Yin L. Y. and Patterson C. (1999) Identification of CHIP, a novel tetratricopeptide repeat-containing protein that interacts with heat shock proteins and negatively regulates chaperone functions. *Mol. Cell. Biol.* **19**, 4535–4545.

Connell P., Ballinger C. A., Jiang J., Wu Y., Thompson L. J., Hohfeld J. and Patterson C. (2001) The co-chaperon CHIP regulates protein triage decisions mediated by heat-shock proteins. *Nat. Cell Biol.* **3**, 93–96.

Dai Q., Zhang C., Wu Y. *et al.* (2003) CHIP activates HSF1 and confers protection against apoptosis and cellular stress. *EMBO J.* **22**, 5446–5458.

Dickson D. W., Lin W. K., Ksiezak-Reding H. and Yen S.-H. (2000) Neuropathologic and molecular considerations. *Adv. Neurol.* **82**, 9–27.

Dou F., Netzer W. J., Tanemura K., Li F., Hartl F. U., Takashima A., Gouras G. K., Greengard P. and Xu H. (2003) Chaperons increase association of tau protein with microtubules. *Proc. Natl Acad. Sci. USA* **100**, 721–726.

Gong C.-X., Liu F., Grundke-Iqbal I. and Iqbal K. (2005) Post-translational modification of tau protein in Alzheimer's disease. *J. Neural. Transm.* **112**, 813–838.

Grundke-Iqbal I., Iqbal K., Quinlan M., Tung Y. C., Zaidi M. S. and Wisniewski H. M. (1986) Microtubule-associated protein tau: a component of Alzheimer-paired helical filaments. *J. Biol. Chem.* **261**, 6084–6089.

Hatakeyama S., Yada M., Matsumoto M., Ishida N. and Nakayama K. I. (2001) U box proteins as a new family of ubiquitin-protein ligases. *J. Biol. Chem.* **276**, 33111–33120.

Hatakeyama S., Matsumoto M., Kamura T., Murayama M., Chui D.-H., Planel E., Takahashi R., Nakayama K. I. and Takashima A. (2004) U-box protein carboxyl terminus of Hsc70-interacting protein (CHIP) mediates poly-ubiquitylation preferentially on four-repeat tau and is involved in neurodegeneration of tauopathy. *J. Neurochem.* **91**, 299–307.

Imai Y., Soda M., Hatakeyama S., Akagi T., Hashikawa T., Nakayama K. and Takahashi R. (2002) CHIP is associated with Parkin, a gene responsible for familial Parkinson's disease, and enhances its ubiquitin ligase activity. *Mol. Cell* **10**, 55–67.

Ishihara T., Hong M., Zhang B., Nakagawa Y., Lee M. K., Trojanowski J. Q. and Lee V. M.-Y. (1999) Age-dependent emergence and progression of a tauopathy in transgenic mice overexpressing the shortest human tau isoform. *Neuron* **24**, 751–762.